Electronic Supplementary Material (ESI) for Organic & Biomolecular Chemistry.

Supplementary Information

On the potential intermediacy of $PhIBr_2$ as a brominating agent

Tania, Andrew Molino, Lachlan Sharp-Bucknall, David J. D. Wilson*, and Jason L. Dutton*

Department of Biochemistry and Chemistry, La Trobe Institute for Molecular Science, La Trobe University, Melbourne 3086, Australia

j.dutton@latrobe.edu.au

Experimental Section

1.1 Experimental Details

All reagents were purchased from Sigma Aldrich and used as received. Solvents were dried using an Innovative Technologies Solvent Purification System. The dried solvents were stored under N_2 atmosphere over 3 Å molecular sieves in the glovebox. Deuterated solvents for NMR spectroscopy were purchased from Cambridge Isotope Laboratories and dried by stirring for three days over CaH_2, distilled prior to use, and stored in the glovebox over 3 Å molecular sieves. All reactions were performed within a N_2 filled glove box unless otherwise stated. Glassware was dried in an oven at 120 °C overnight and transferred to the glovebox port or Schlenk line where it was subjected to three vacuum cycles over 30 minutes prior to use. NMR spectra for all experiments were recorded using Bruker Ultrashield Plus 500 MHz and Ascend 400 MHz spectrometers. The UV-Vis absorptions were recorded using Agilent Technology Cary 300 UV-Vis spectrophotometer. The abbreviations used to report NMR signal multiplicity are s = singlet, d = doublet, t = triplet, m = multiplet. Other abbreviations used are PIFA = $PhI(OTFA)_2$, PIDA = $PhI(OAc)_2$.

1.2 Experimental Methods

a. Synthesis of PIFA

In accordance with procedure reported by Silverio et al,[1] an RBF was charged with PIDA (5 g, 15.5 mmol) under N_2. Trifluoroacetic acid (TFA, 8 mL, 104.5 mmol) was added dropwise to this solid while stirring. This reaction mixture was then heated up to 55 °C and stirred for 1 hour under N_2. After 1 hour, a suspension with white solid was observed. TFA (4 mL) was added dropwise to this suspension to afford a clear solution. The RBF was then placed over an ice bath to cool reaction mixture to 0 °C. A white crystalline solid precipitated out of the solution. The precipitates were filtered via vacuum filtration and washed with pentane. After drying under vacuum, title compound (5 g, 11.6 mmol, 75% yield) was obtained as a white crystalline solid. The spectral data was consistent with that previously reported.[1]

^{1}H NMR (400 MHz, $CDCl_3$): δ 8.18-8.21 (d, 2H), 7.73-7.76 (t, 1H), 7.60-7.64 (d, 2H)

^{19}F NMR (400 MHz, $CDCl_3$): δ -73.4 (s)

b. Reaction of PIFA with TMSBr

Following the procedure reported by Cossio and Vallribera,[2] PIFA (50 mg, 0.116 mmol) was dissolved in 500 µL $CDCl_3$ in a reaction vial in glove box. A clear solution was formed. TMSBr (18 mg, 0.116 mmol) was added to this solution. The solution turned orange immediately. The reaction contents were transferred to an NMR tube. The NMR was recorded.

c. Reaction of PIFA with 2 equivalents of TMSBr

Following the procedure reported by Cossio and Vallribera,[2] PIFA (50 mg, 0.116 mmol) was dissolved in 500 µL $CDCl_3$. TMSBr (36 mg, 0.232 mmol) was added to this solution. The solution turned orange immediately. The reaction contents were transferred to an NMR tube to record NMR. This experiment was also repeated in CD_2Cl_2.

d. Reaction of PIDA with TMSBr

Following the procedure reported by Cossio and Vallribera,[2] PIDA (50 mg, 0.157 mmol) was dissolved in 500 µL $CDCl_3$. TMSBr (12 mg, 0.157 mmol) was added to this clear solution. The solution turned orange gradually. The reaction contents were transferred to an NMR tube to record NMR.

e. Reaction of PIDA with 2 equivalents of TMSBr

Following the procedure reported by Cossio and Vallribera,[2] PIDA (50 mg, 0.157 mmol) was dissolved in 500 µL $CDCl_3$. TMSBr (24 mg, 0.314 mmol) was added to this solution. The solution turned orange immediately. The reaction contents were transferred to an NMR tube to record NMR. This experiment was also repeated in CD_2Cl_2.

f. Reaction of PhI with Br_2

Following the procedure reported by Fryberg,[3] reaction vial was charged with PhI (22 µL, 0.2 mmol) in 1 mL dry hexane. Br_2 (10 µL, 0.2 mmol) was added to this solution at room temperature to afford an orange solution. This solution was then cooled to -5 °C. A variable temperature NMR experiment was performed to record NMR spectrum of reaction mixture at -5 °C, -1 °C, 12 °C and 25 °C.

g. Bromination of aryl substrates using Br_2

A reaction vial was charged with Br_2 (10 µL, 0.2 mmol) in 2 mL dry CH_2Cl_2 under N_2. While stirring, 1 equivalent of aryl substrate was added. The reaction mixture was left to stir over-night and the reaction mixture was poured into water. The CH_2Cl_2 extract was collected and dried over $MgSO_4$. The dried filtrate was subject to vacuum on rotavap. The obtained crude product was dissolved in 500 µL of $CDCl_3$ for recording NMR.

This experiment was also repeated at NMR scale by dissolving 0.2 mmol of aryl substrate in 500 µL $CDCl_3$. 0.2 mmol of Br_2 was added to this solution and reaction was transferred to an NMR tube to record chemical shifts without work up.

h. Bromination of aryl substrates using PIFA/2 TMSBr

A reaction vial was charged with PIFA (85 mg, 0.2 mmol) in 500 µL $CDCl_3$. TMSBr (62 mg, 0.4 mmol) was added to afford an orange-coloured solution. 1 equivalent of aryl substrate was added to this reaction mixture. This mixture was then transferred to an NMR tube to record NMR spectrum.

i. Reaction of PIDA and NaBr

Following the procedure reported by Karade,[4] PIDA (50 mg, 0.157 mmol) was dissolved in 500 µL MeOD. NaBr (32 mg, 0.314 mmol) was added to this clear solution. The solution turned bright yellow immediately. The reaction contents were transferred to an NMR tube to record the NMR spectrum.

j. Reaction of PIDA and NaBr with Benzaldehyde

Following the procedure reported by Karade,[4] a reaction flask was charged with benzaldehyde (106 mg, 1 mmol) and NaBr (205 mg, 2 mmol) in 15 mL MeOH. PIDA (322 mg, 1 mmol) was added to this clear solution while stirring. The solution turned bright yellow gradually. After 2 hours of stirring, 10 mL H_2O was added. The product was extracted using DCM and dried over $MgSO_4$. The solvent was removed under vacuum to obtain crude product. This product was then dissolved in $CDCl_3$ to record NMR.

k. Reaction of Br_2 with Benzaldehyde

A reaction flask was charged with benzaldehyde (106 mg, 1 mmol) and Br_2 (159 mg, 1 mmol) in 15 mL MeOH. The solution turned bright orange. After 2 hours of stirring, 10 mL H_2O was added. The product was extracted using DCM and dried over $MgSO_4$. The solvent was removed under vacuum to obtain crude product. This product was then dissolved in $CDCl_3$ to record NMR. This experiment was also repeated in presence of PhI.

l. Reaction of PIDA and [NBu_4][Br]

Following the procedure reported by Uchiyama,[5] PIDA (14 mg, 0.04 mmol) was dissolved in 500 µL CD_2Cl_2. [NBu_4][Br] (14 mg, 0.04 mmol) was added to this clear solution. The solution turned bright yellow gradually. The reaction contents were transferred to an NMR tube to record the NMR spectrum. ESI/MS was recorded for reaction aliquot in negative polarity.

m. Reaction of PIDA and [$NHex_4$][Br]

Following the procedure reported by Uchiyama,[5] PIDA (14 mg, 0.04 mmol) was dissolved in 500 µL CH_2Cl_2. [$NHex_4$][Br] (21 mg, 0.04 mmol) was added to this clear solution. The solution turned bright yellow gradually. ESI/MS was recorded for resulting solution in negative polarity.

n. Immediately monitored reactions of PIFA/TMSBr and Br_2 with anisole.

i. PIFA/2 TMSBr

An NMR tube was charged with a solution of PIFA (41.6 mg, 0.097 mmol) and TMSBr (32 mg, 0.21 mmol) in 500 µL $CDCl_3$ and inverted several times to reach homogeneity. After allowance of 3 minutes reaction time, anisole (10.5, µL 0.98 mmol) was then added and the tube was again inverted several times. ^{1}H NMR spectra were obtained within 5 minutes.

ii. Br_2

To an NMR tube charged with 500 µL $CDCl_3$ was added Br_2 (15 µL, 0.291 mmol) which was inverted several times to homogeneity. Anisole (31.5 µL, 0.294 mmol) was then added and the tube was again inverted several times. ^{1}H NMR spectra were obtained within 5 minutes. This experiment was repeated with 2 equivalents of Br_2 and ^{1}H NMR was recorded.

o. Reference NMR chemical shifts

PhI: Commercial Sample

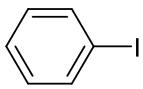

^{1}H NMR (500 MHz, $CDCl_3$) δ 7.70-7.71 (d, 2H), 7.32-7.35 (t, 1H), 7.09-7.12 (t, 2H)

Phenyl iodo bis(trifluoroacetate) (PIFA): Synthesised using reported procedure.[1]

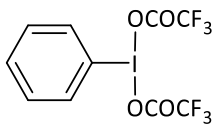

^{1}H NMR (400 MHz, $CDCl_3$) δ 8.18-8.21 (d, 2H), 7.73-7.76 (t, 1H), 7.60-7.64 (t, 2H)

^{19}F NMR (400 MHz, $CDCl_3$) δ -73.4 (s)

Phenyl iodo diacetate (PIDA): Commercial sample

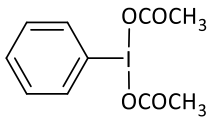

^{1}H NMR (400 MHz, $CDCl_3$) δ 8.07-8.09 (d, 2H), 7.57-7.61 (t,1H), 7.47-7.51 (t, 2H)

Anisole: Commercial sample

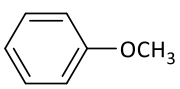

^{1}H NMR (400 MHz, $CDCl_3$) δ 7.35-7.39 (t, 2H), 7.01-7.04 (t, 1H), 6.97-7.00 (t, 2H), 3.86 (s, 3H)

p-Bromo anisole: Commercial sample

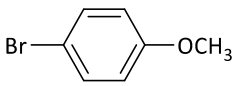

^{1}H NMR (400 MHz, $CDCl_3$) δ 7.37-7.39 (d, 2H), 6.78-6.80 (d, 2H), 3.80 (s, 3H)

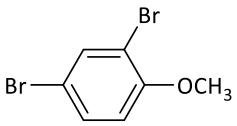

o,p-dibromo anisole: Commercial sample

^{1}H NMR (400 MHz, $CDCl_3$) δ 7.67-7.66 (s, 1H), 7.37-7.39 (d, 1H), 6.76-6.78 (d, 1H), 3.87 (s, 3H)

1,3,5-Trimethoxybenzene: Commercial sample

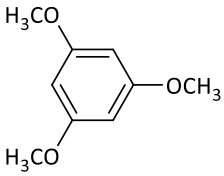

^{1}H NMR (400 MHz, $CDCl_3$) δ 6.09 (s, 3H), 3.77 (s, 9H)

2-Bromo-1,3,5-trimethoxybenzene: Compared with reported chemical shift[6]

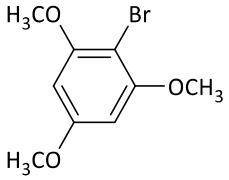

^{1}H NMR (400 MHz, $CDCl_3$) δ 6.17 (s, 2H), 3.88 (s, 6H), 3.82 (s, 3H)

2,6-Dibromo-1,3,5-trimethoxybenzene: Compare with reported chemical shift[6]

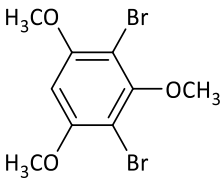

^{1}H NMR (400 MHz, $CDCl_3$) δ 6.36 (s, 1H), 3.91 (s, 6H), 3.87 (s, 3H)

Salicylic Acid: Commercial sample

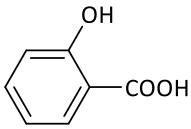

^{1}H NMR (400 MHz, $CDCl_3$) δ 10.38 (s, 1H), 7.93-7.95 (d, 1H), 7.52-7.54 (t, 1H), 7.01-7.03 (d, 1H), 6.93-6.97 (t, 1H)

4-Bromo-2-hyroxybenzoic acid: Compared with reported chemical shift[7]

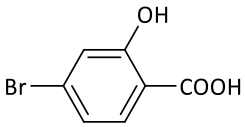

^{1}H NMR (400 MHz, $CDCl_3$) δ 11.71 (s, 1H), 8.05 (s,1H), 7.62-7.63 (d, 1H), 6.92-6.94 (d, 1H)

1,4-dimethoxybenzene: Commercial sample

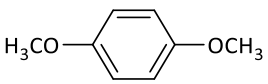

^{1}H NMR (400 MHz, $CDCl_3$) δ 6.85 (s, 4H), 3.78 (s, 6H)

2-Bromo-1,4-dimethoxybenzene: Compared with reported chemical shift[8]

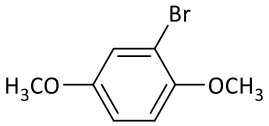

^{1}H NMR (400 MHz, $CDCl_3$) δ 7.10-7.13 (m, 1H), 6.80-6.83 (m, 2H), 3.84 (s, 3H), 3.76 (s, 3H)

Mesitylene: Commercial sample

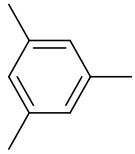

^{1}H NMR (400 MHz, $CDCl_3$) δ 6.78 (s, 3H), 2.26 (s, 9H)

Bromo mesitylene: Compared with reported chemical shift[8]

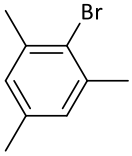

^{1}H NMR (400 MHz, $CDCl_3$) δ 6.88 (s, 2H), 2.36 (s, 6H), 2.23 (s, 3H)

Benzaldehyde: Commercial sample

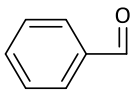

^{1}H NMR (400 MHz, $CDCl_3$) δ 10.00 (s, 1H), 7.86-7.89 (d, 2H), 7.60-7.64 (t, 1H), 7.51-7.54 (t, 2H)

p. UV-Vis Absorption experiments

i. Br_2

In a volumetric flask, a 0.04 M solution of Br_2 was prepared by dissolving Br_2 (10 µL, 0.2 mmol) in 5 mL CH_2Cl_2. This solution was further diluted to prepare several dilutions. These dilutions were used to record absorption from wavelength range 190 nm to 800 nm. This experiment was also repeated using methanol as solvent.

ii. PhI + Br_2

In a volumetric flask, a 0.04 M solution of PhI was prepared by dissolving PhI (42 mg, 0.2 mmol) in 5 mL CH_2Cl_2. Br_2 (10 µL, 0.2 mmol) was added to this solution to form an orange solution. This solution was further diluted to prepare several dilutions. These dilutions were used to record absorption from wavelength range 190 nm to 800 nm. This experiment was also repeated using methanol as solvent.

iii. PIFA + TMSBr in CH_2Cl_2

In a volumetric flask, a 4 mM solution of PIFA was prepared by dissolving PIFA (17.2 mg, 0.04 mmol) in 10 mL CH_2Cl_2. TMSBr (6.12 mg, 0.04 mmol) was added to this solution to form an orange solution. This solution was further diluted to prepare several dilutions. These dilutions were used to record absorption from wavelength range 190 nm to 800 nm.

iv. PIFA + 2 TMSBr in CH_2Cl_2

In a volumetric flask, a 4 mM solution of PIFA was prepared by dissolving PIFA (17.2 mg, 0.04 mmol) in 10 mL CH_2Cl_2. TMSBr (12.2 mg, 0.08 mmol) was added to this solution to form an orange solution. This solution was used to record absorption from wavelength range 190 nm to 800 nm over time.

v. PIDA + 2 NaBr in MeOH

In a volumetric flask, a 0.04 M solution of PIDA was prepared by dissolving PIDA (64 mg, 0.2 mmol) in 5 mL MeOH. NaBr (41 mg, 0.4 mmol) was added to this solution to form a bright yellow solution. This solution was further diluted to prepare several dilutions. These dilutions were used to record absorption from wavelength range 190 nm to 800 nm.

1.3 NMR Investigations

a. PhI

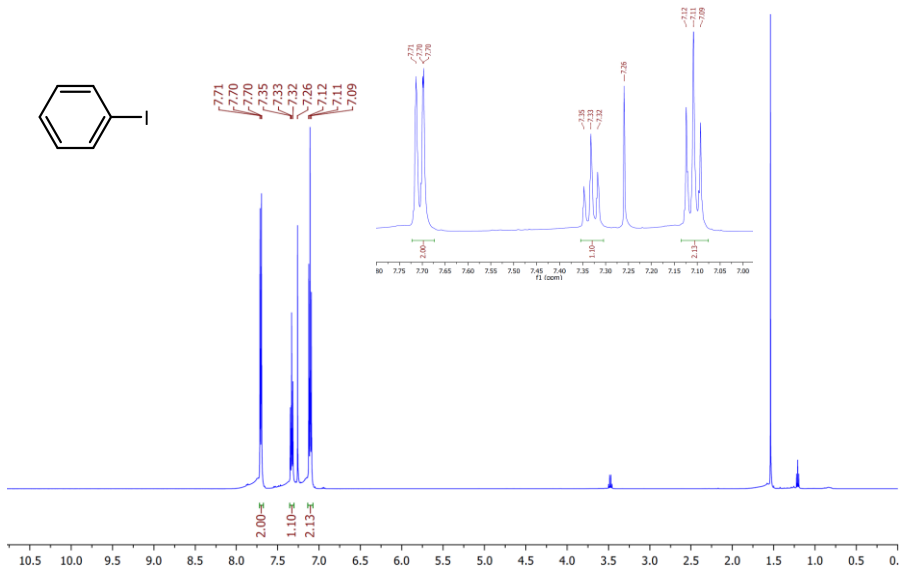

Figure S1: ^{1}H NMR spectrum of PhI in $CDCl_3$ (inset) aryl region of the spectrum.

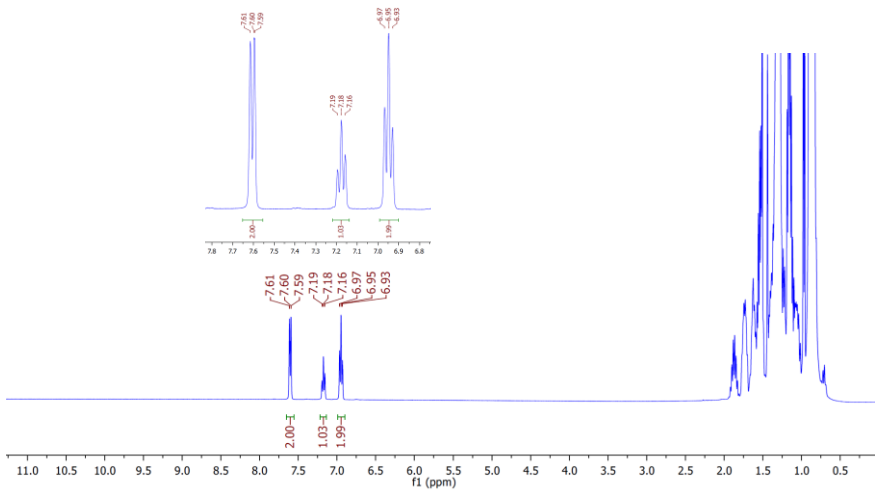

Figure S2: ^{1}H NMR spectrum of PhI in hexane (inset) aryl region of the spectrum.

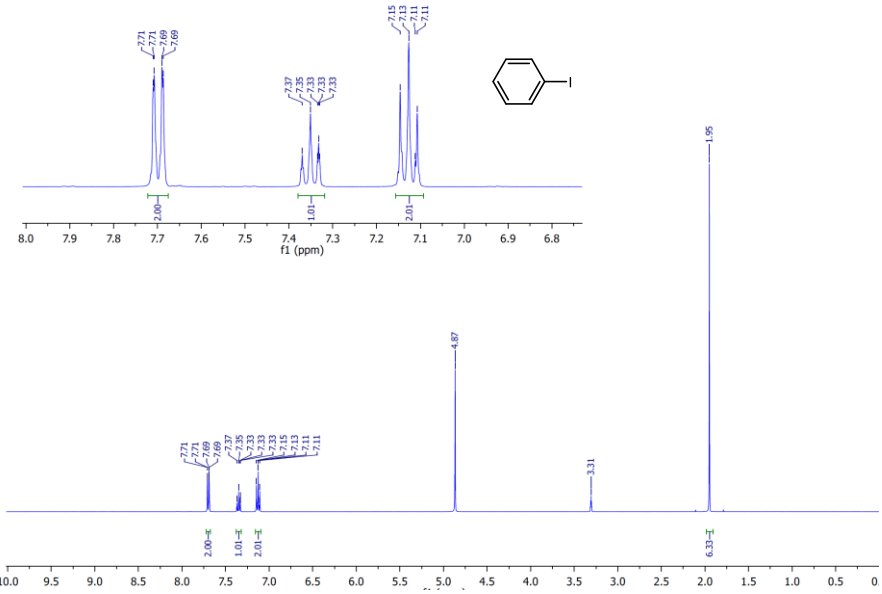

Figure S3: ^{1}H NMR spectrum of PhI in MeOD (inset) aryl region of the spectrum.

b. PhI+ Br_2

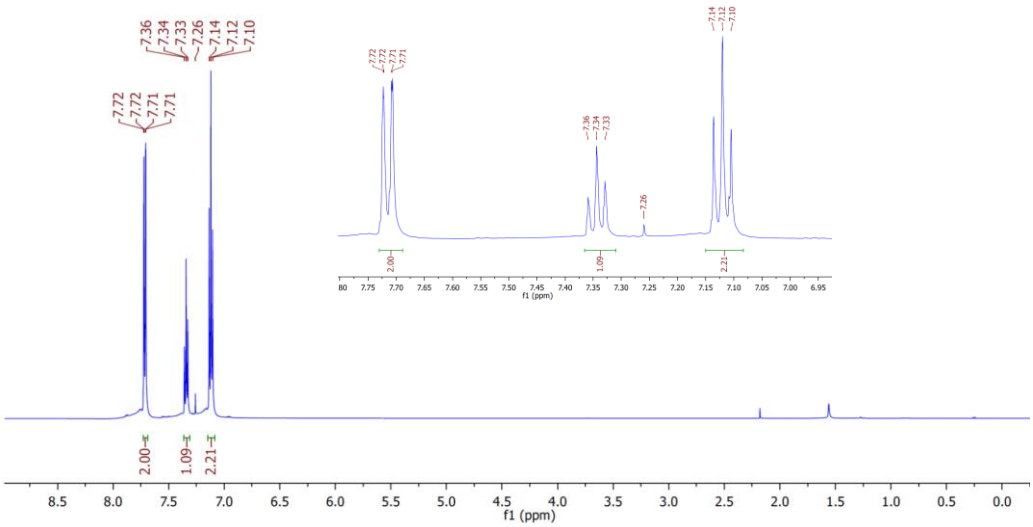

Figure S4: ^{1}H NMR spectrum of PhI and Br_2 in $CDCl_3$ (inset) aryl region of spectrum.

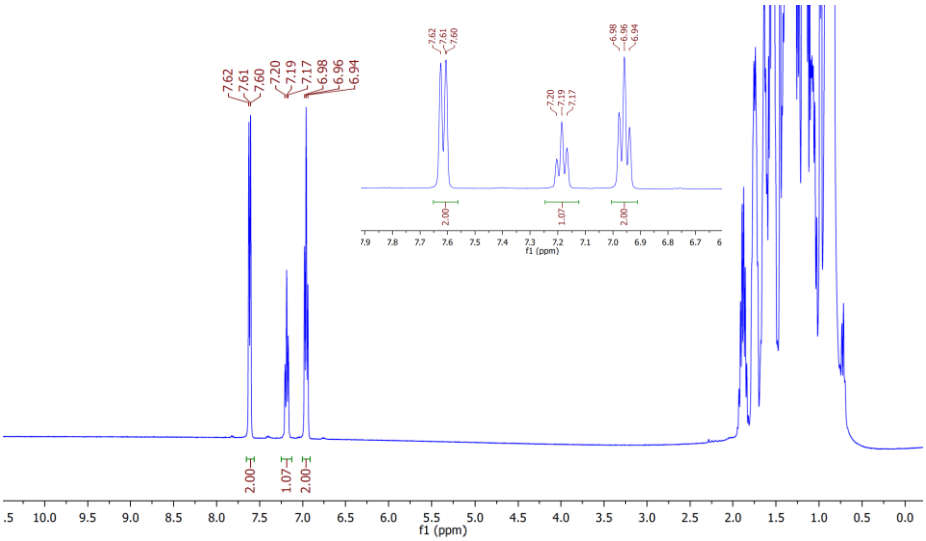

Figure S5: ^{1}H NMR spectrum of PhI and Br_2 in hexane (inset) aryl region of spectrum.

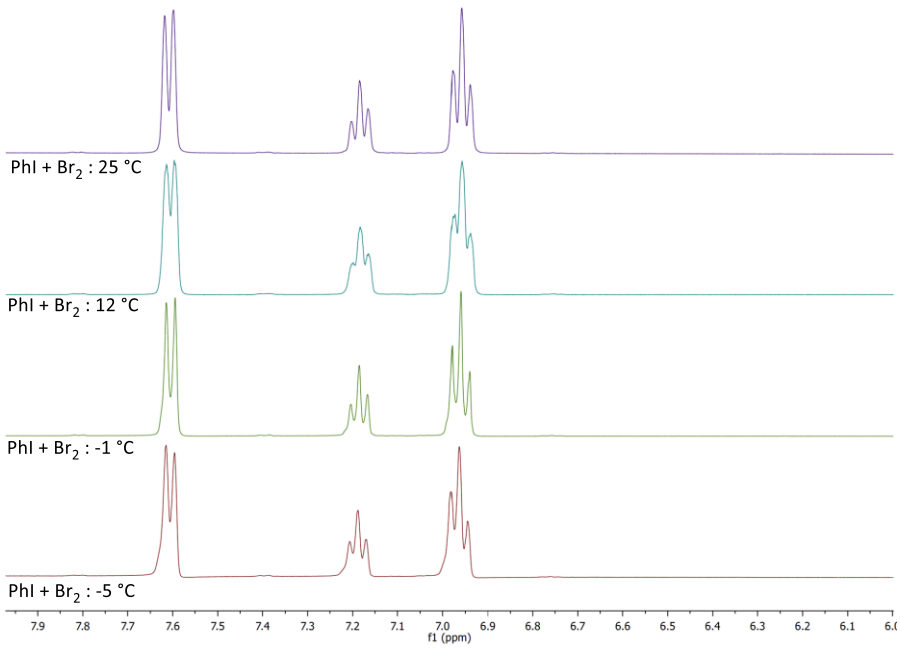

Figure S6: ^{1}H NMR spectra stack of PhI and Br_2 in hexane at variable temperatures (top to bottom) i. 25 °C ii. 12 °C iii. -1 °C and iv. -5 °C.

c. PIFA

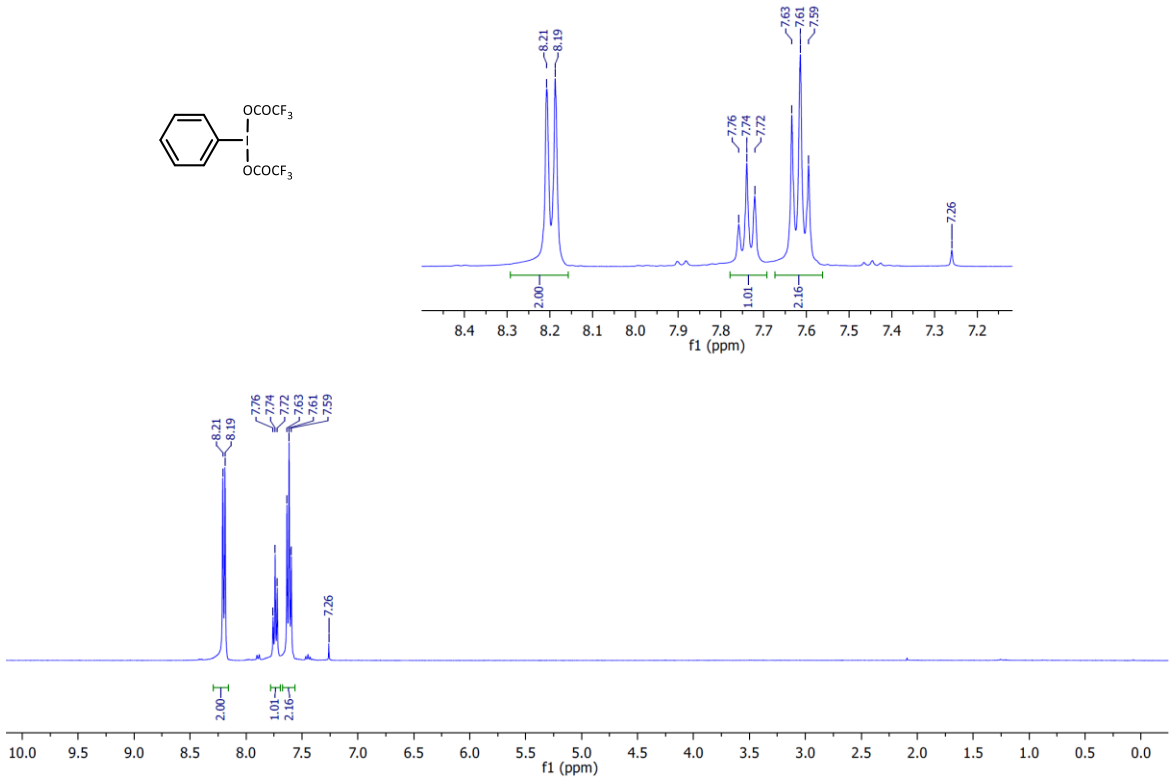

Figure S7: ^{1}H NMR spectrum of PIFA in $CDCl_3$ (inset) aryl region of spectrum.

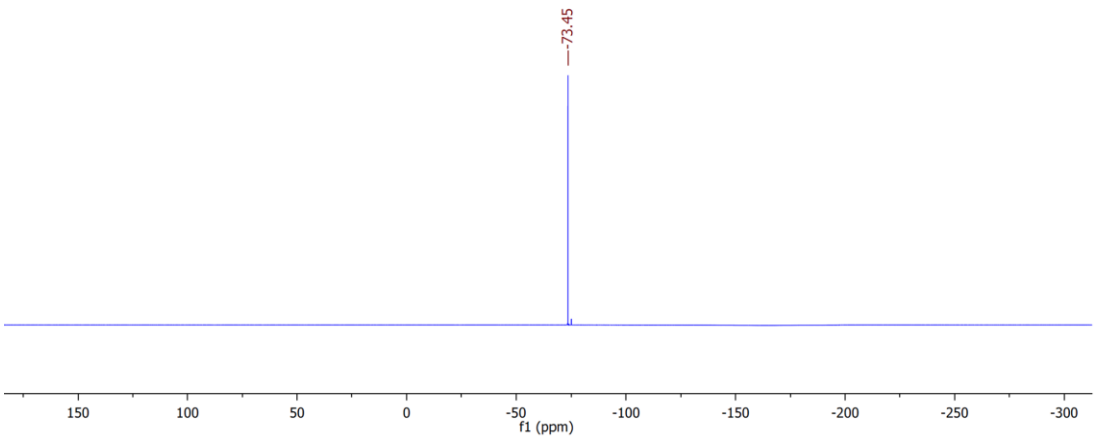

Figure S8: ^{19}F NMR spectrum of PIFA in $CDCl_3$.

d. PIFA + x TMSBr

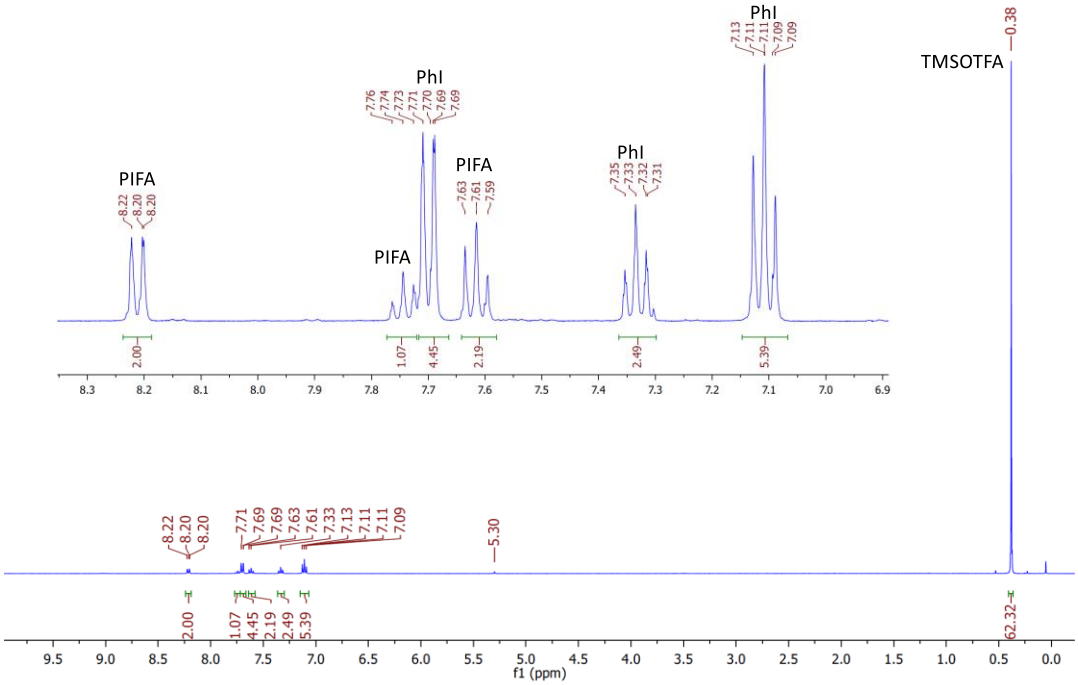

Figure S9: ^{1}H NMR spectrum of PIFA and 2 equivalents of TMSBr in CD_2Cl_2 (inset) aryl region of spectrum with peaks labelled to corresponding compound.

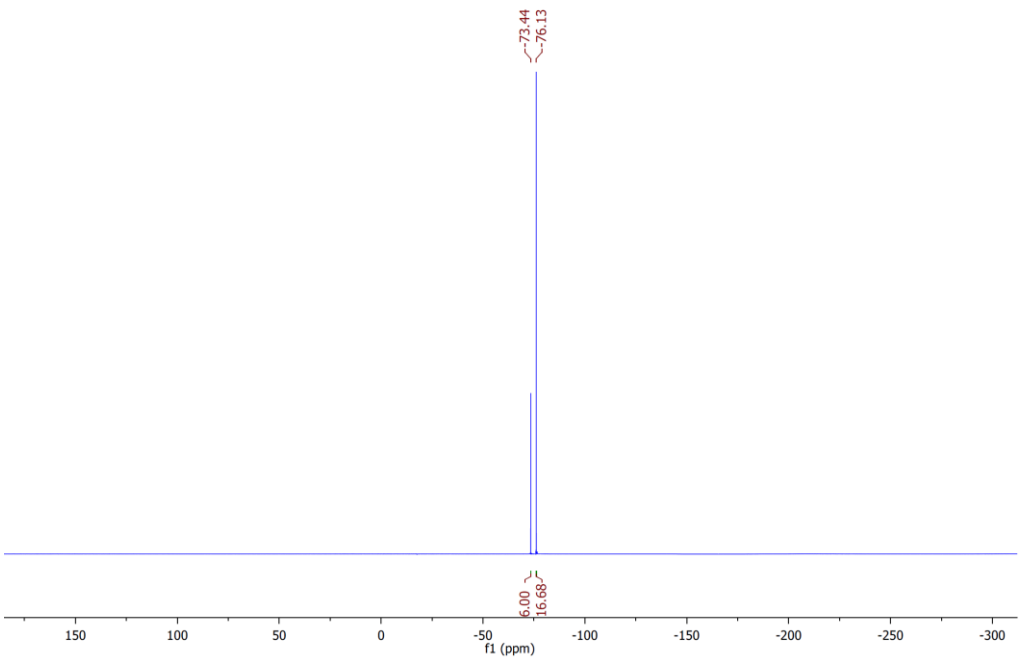

Figure S10: ^{19}F NMR spectrum of PIFA and 2 equivalents of TMSBr in CD_2Cl_2.

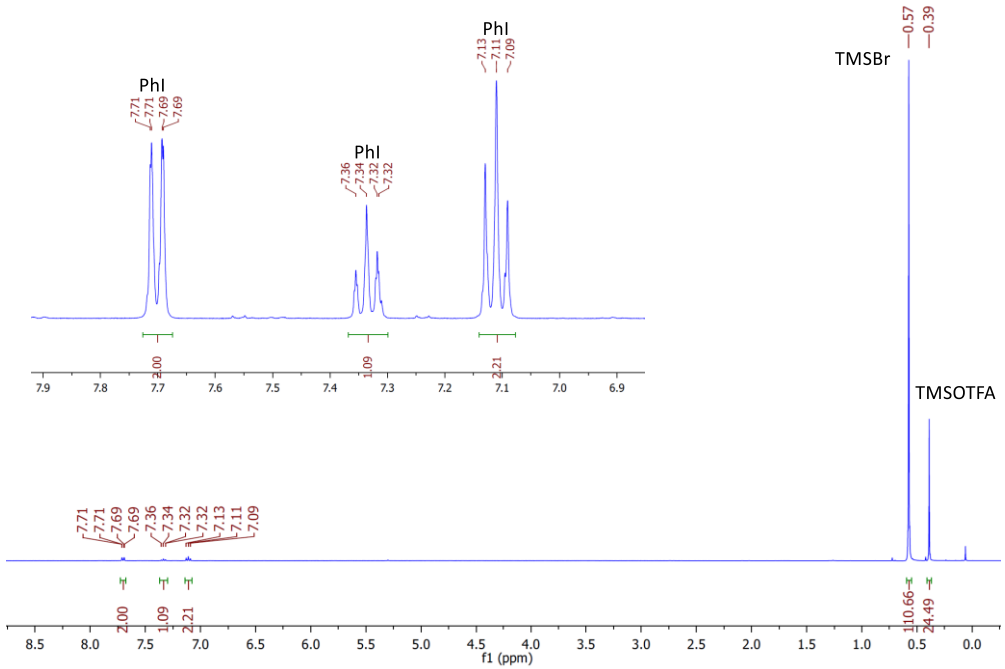

Figure S11: ^{1}H NMR spectrum of PIFA and excess TMSBr in CD_2Cl_2 (inset) aryl region of spectrum with peaks labelled to corresponding compound.

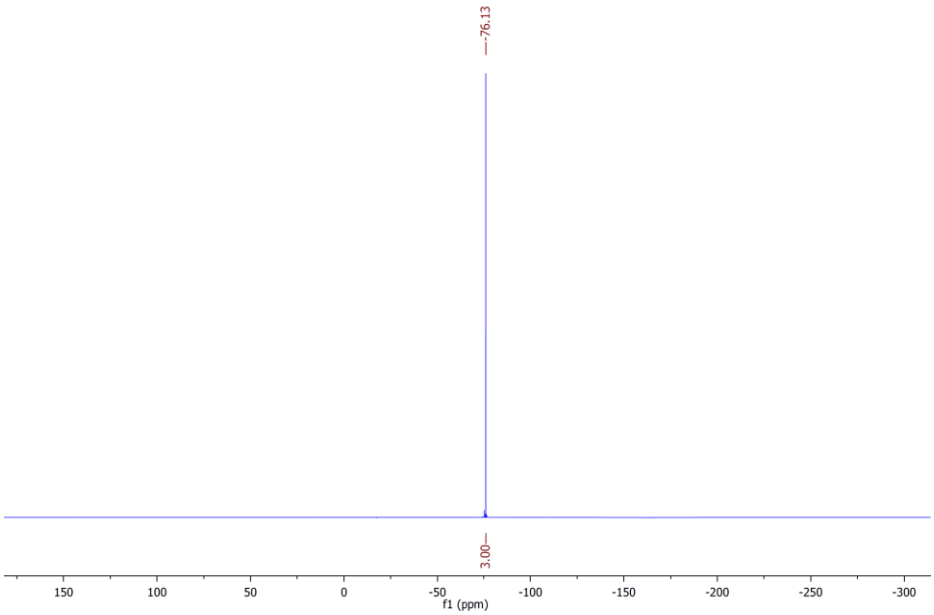

Figure S12: ^{19}F NMR spectrum of PIFA and excess TMSBr in CD_2Cl_2.

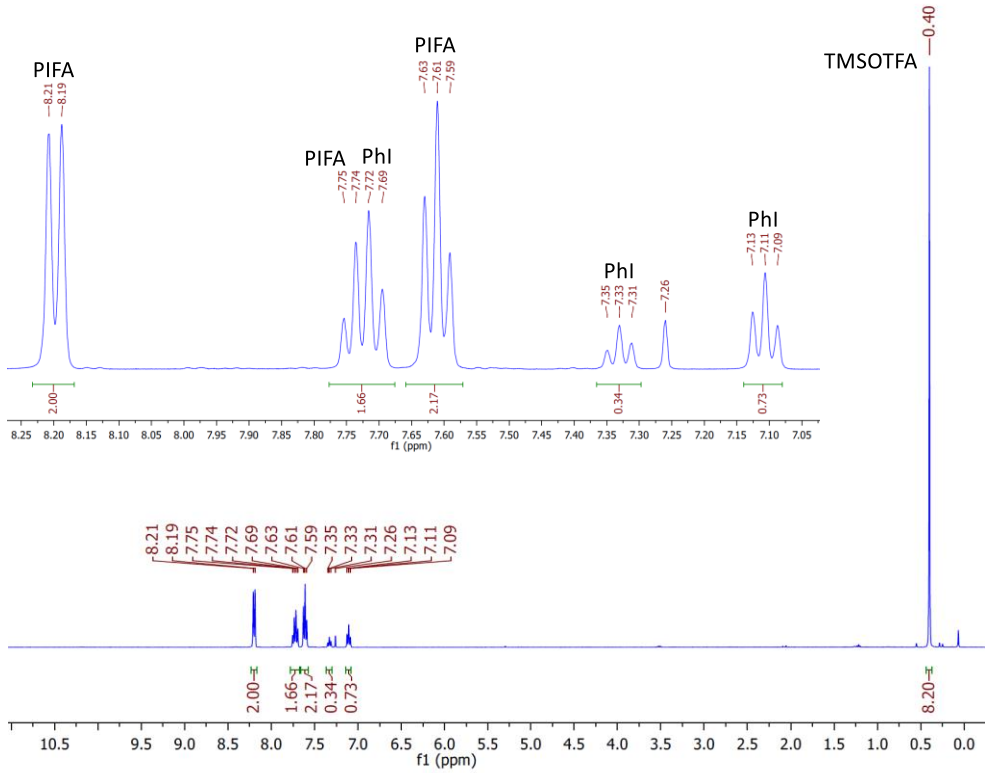

Figure S13: ^{1}H NMR spectrum of PIFA and 1 equivalent of TMSBr in $CDCl_3$ (inset) aryl region of spectrum with peaks labelled to corresponding compound.

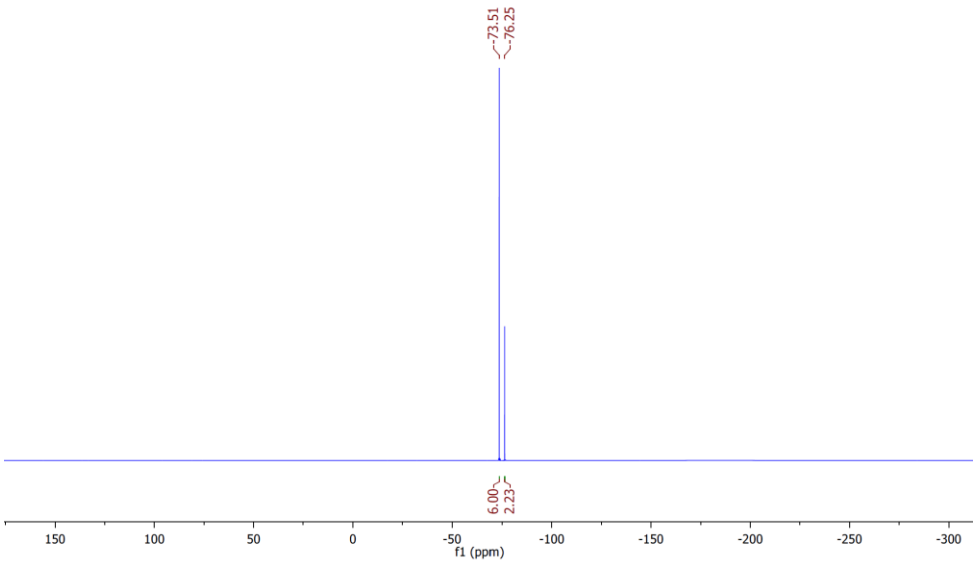

Figure S14: ^{19}F NMR spectrum of PIFA and 1 equivalent of TMSBr in $CDCl_3$.

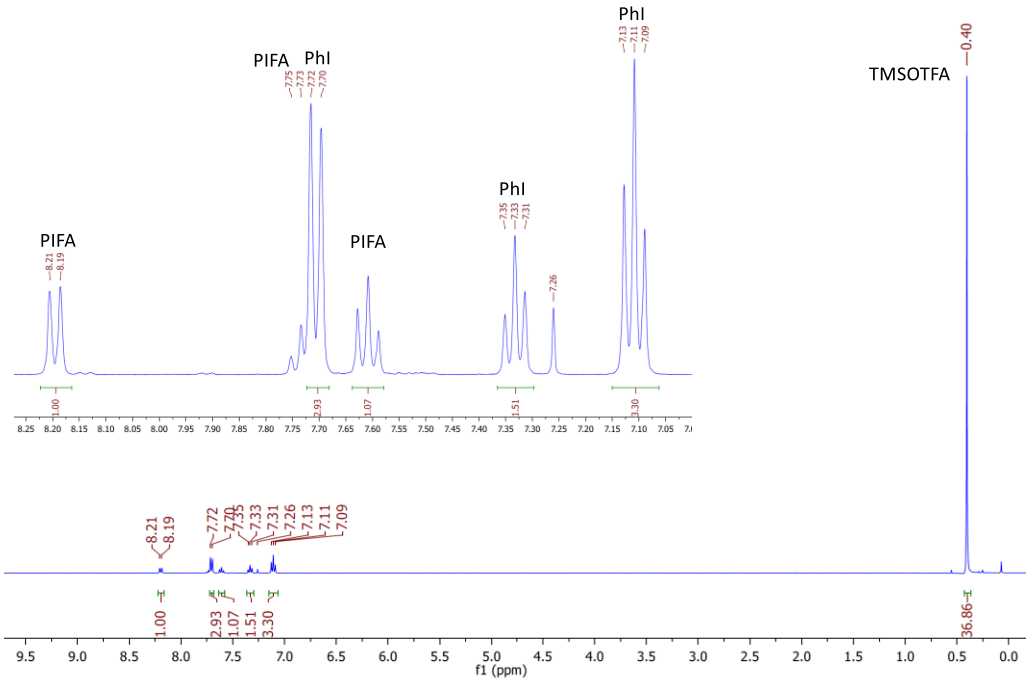

Figure S15: ^{1}H NMR spectrum of PIFA and 2 equivalents of TMSBr in $CDCl_3$ (inset) aryl region of spectrum with peaks labelled to corresponding compound.

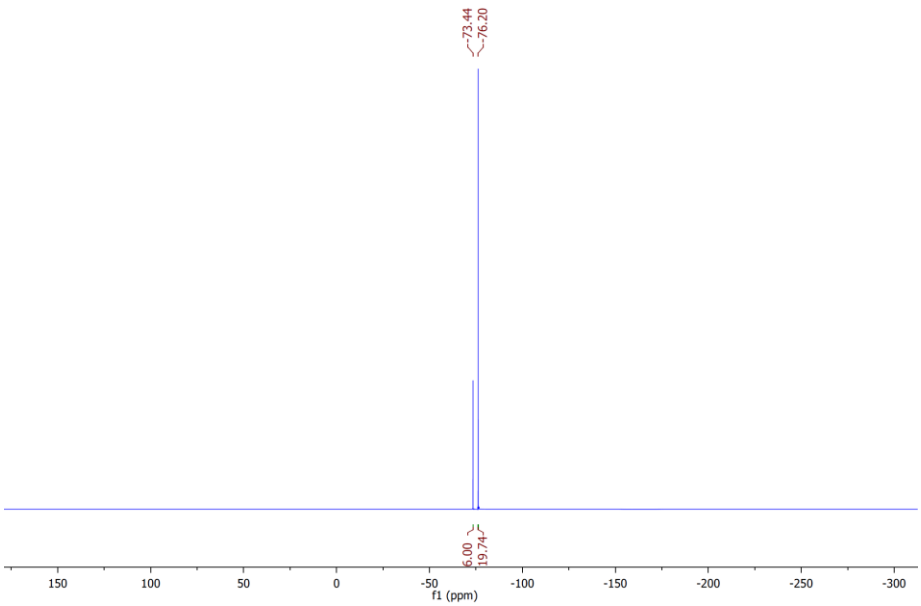

Figure S16: ^{19}F NMR spectrum of PIFA and 2 equivalents of TMSBr in $CDCl_3$.

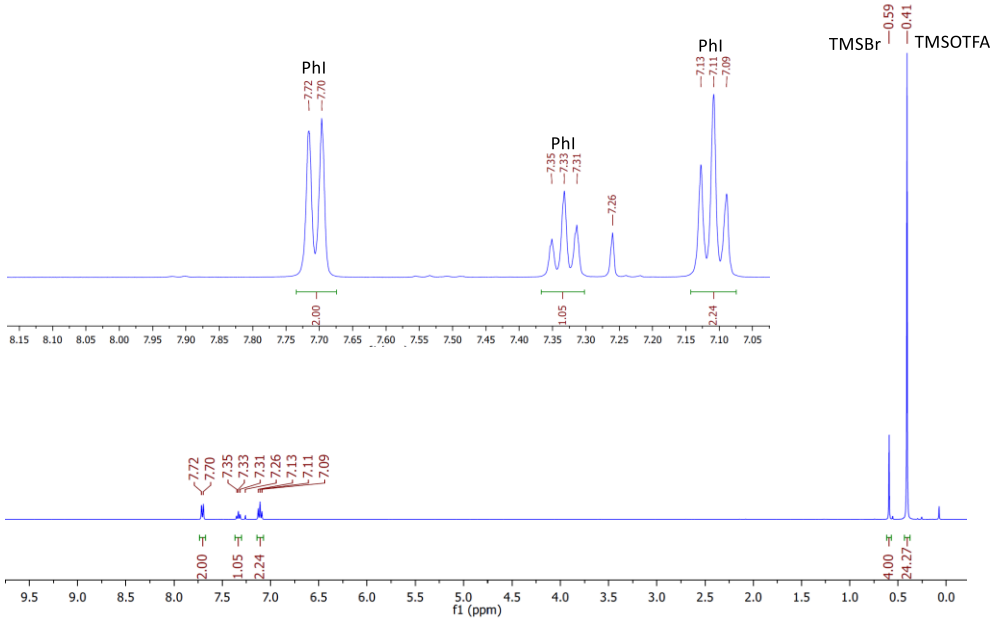

Figure S17: ^{1}H NMR spectrum of PIFA and 3 equivalents of TMSBr in $CDCl_3$ (inset) aryl region of spectrum with peaks labelled to corresponding compound.

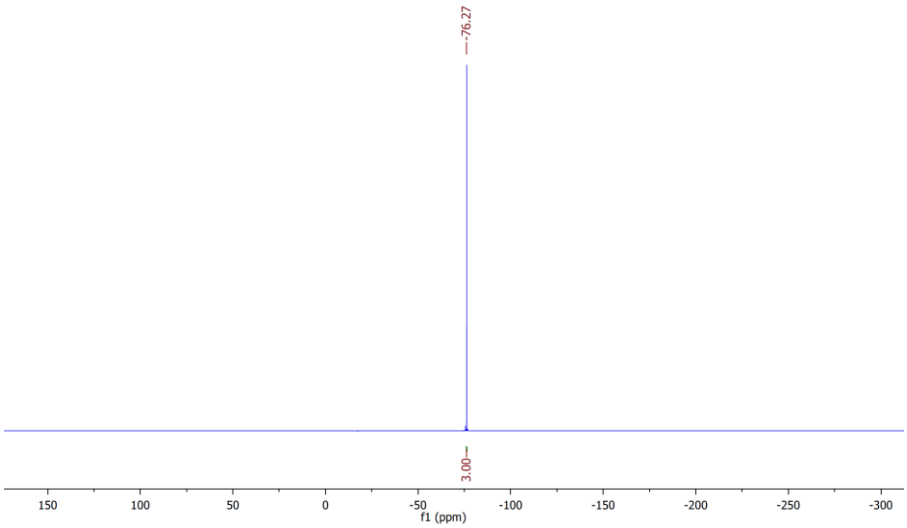

Figure S18: ^{19}F NMR spectrum of PIFA and 3 equivalents of TMSBr in $CDCl_3$.

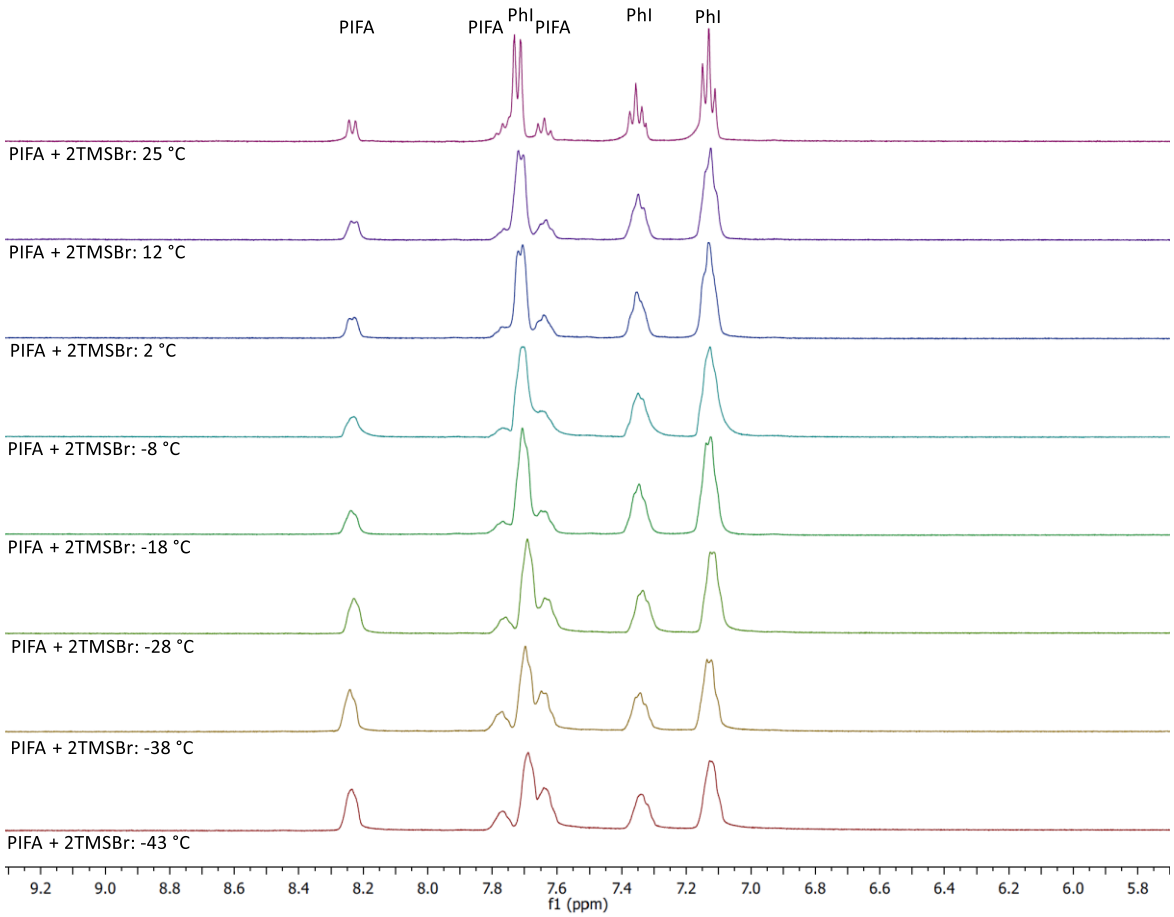

Figure S19: ^{1}H NMR spectra stack of PIFA and 2 equivalents of TMSBr in CD_2Cl_2 at variable temperatures (top to bottom) i. 25 °C ii. 12 °C iii. 2 °C iv. -8 °C v. -18 °C vi. -28 °C vii. -38 °C and viii. -43 °C.

e. PIDA + 2TMSBr

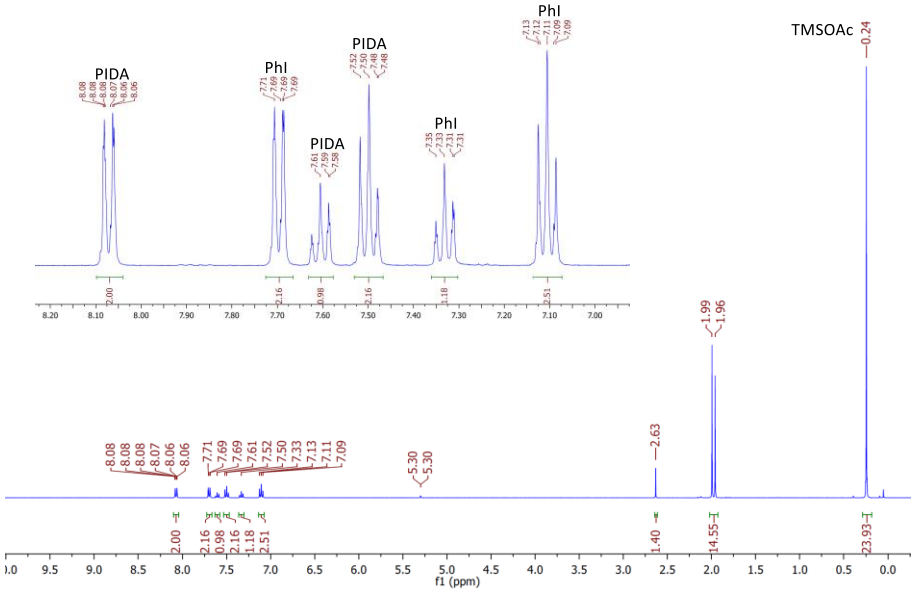

Figure S20: ^{1}H NMR spectrum of PIDA and 2 equivalents of TMSBr in CD_2Cl_2 (inset) aryl region of spectrum with peaks labelled to corresponding compound.

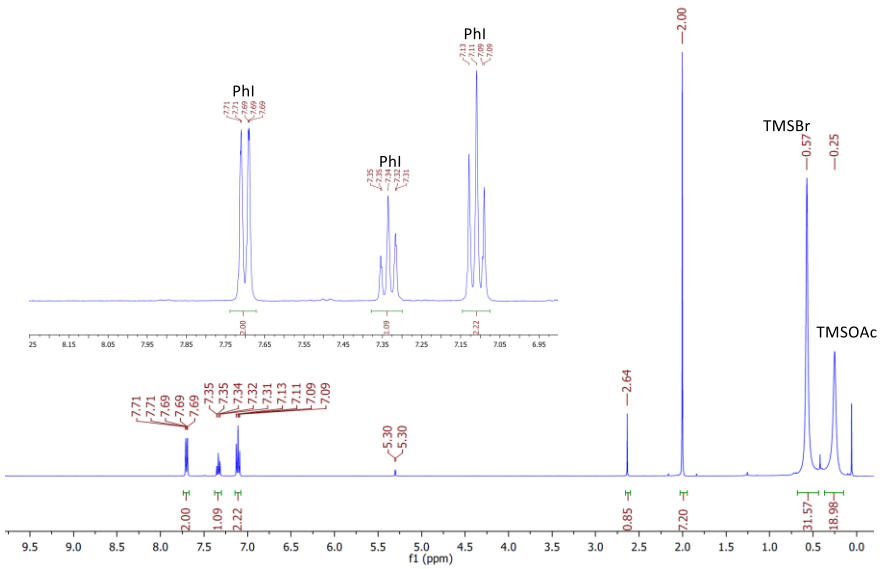

Figure S21: ^{1}H NMR spectrum of PIDA and excess TMSBr in CD_2Cl_2 (inset) aryl region of spectrum with peaks labelled to corresponding compound.

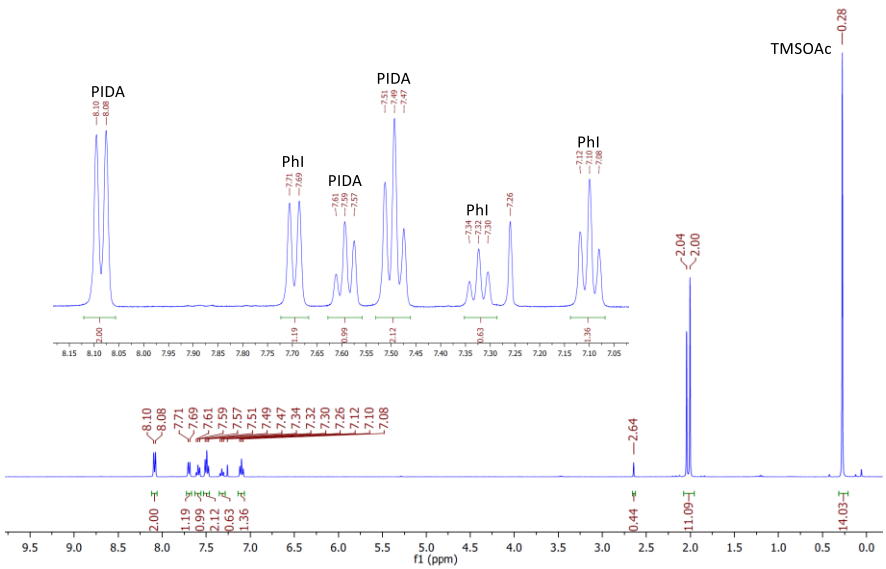

Figure S22: ^{1}H NMR spectrum of PIDA and 1 equivalent of TMSBr in $CDCl_3$ (inset) aryl region of spectrum with peaks labelled to corresponding compound.

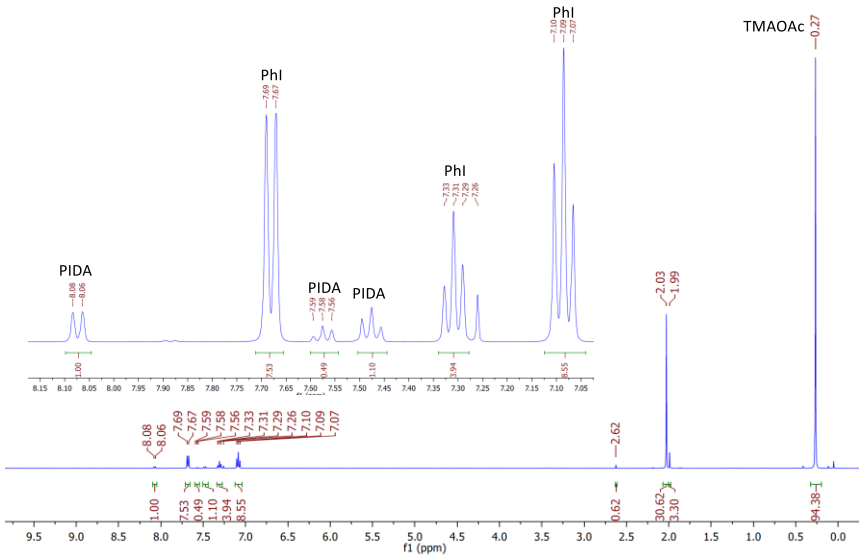

Figure S23: ^{1}H NMR spectrum of PIDA and 2 equivalents of TMSBr in $CDCl_3$ (inset) aryl region of spectrum with peaks labelled to corresponding compound.

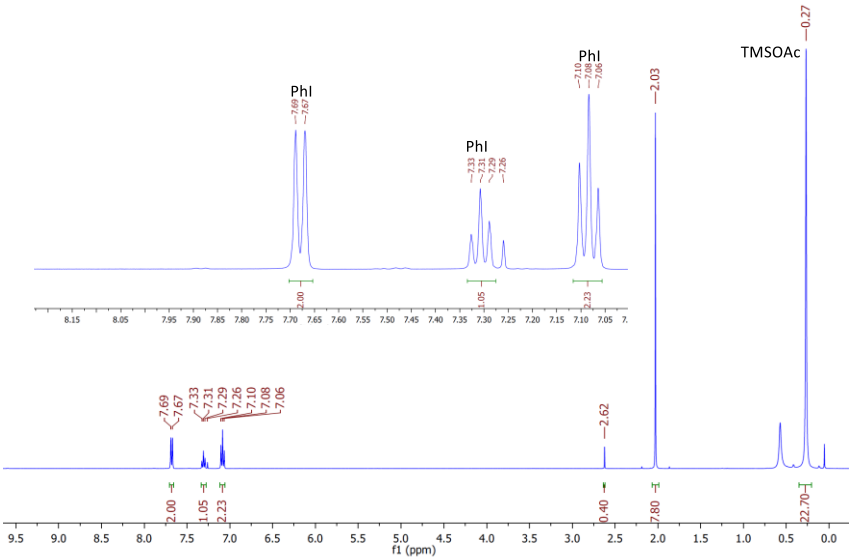

Figure S24: ^{1}H NMR spectrum of PIDA and 3 equivalents of TMSBr in $CDCl_3$ (inset) aryl region of spectrum with peaks labelled to corresponding compound.

f. Bromination of anisole

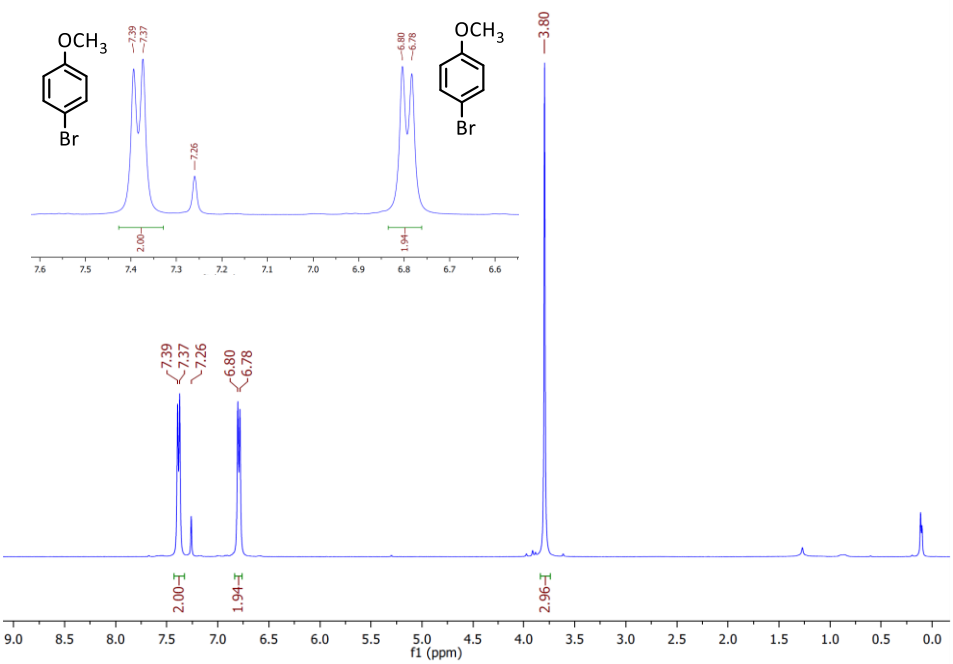

Figure S25: ^{1}H NMR spectrum of reaction of anisole and Br_2 under N_2 in $CDCl_3$ (inset) aryl region of spectrum with peaks labelled to corresponding compound.

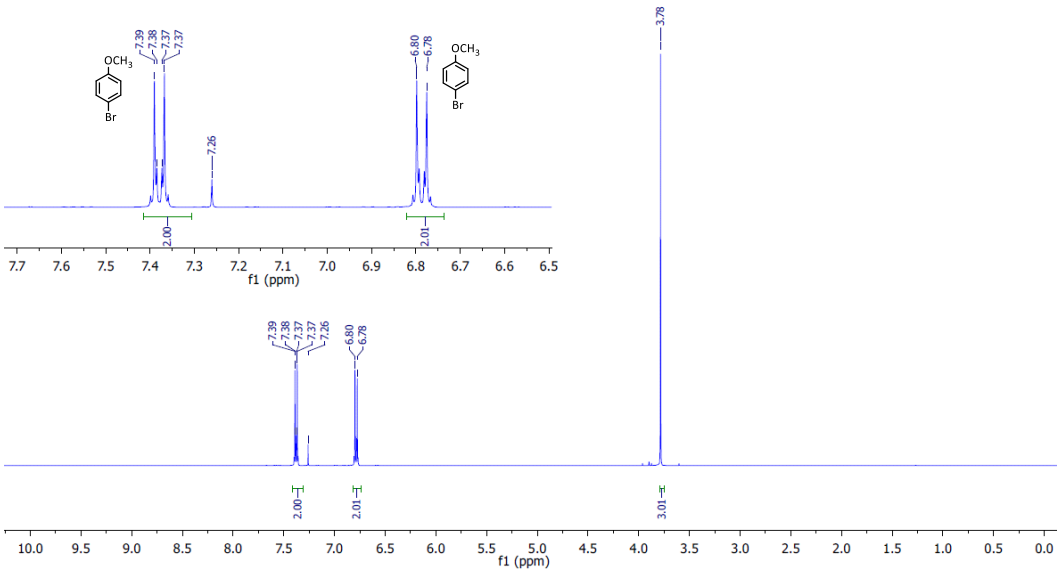

Figure S26: ^{1}H NMR spectrum of reaction of anisole and 2 equivalents of Br_2 in $CDCl_3$ (inset) aryl region of spectrum with peaks labelled to corresponding compound.

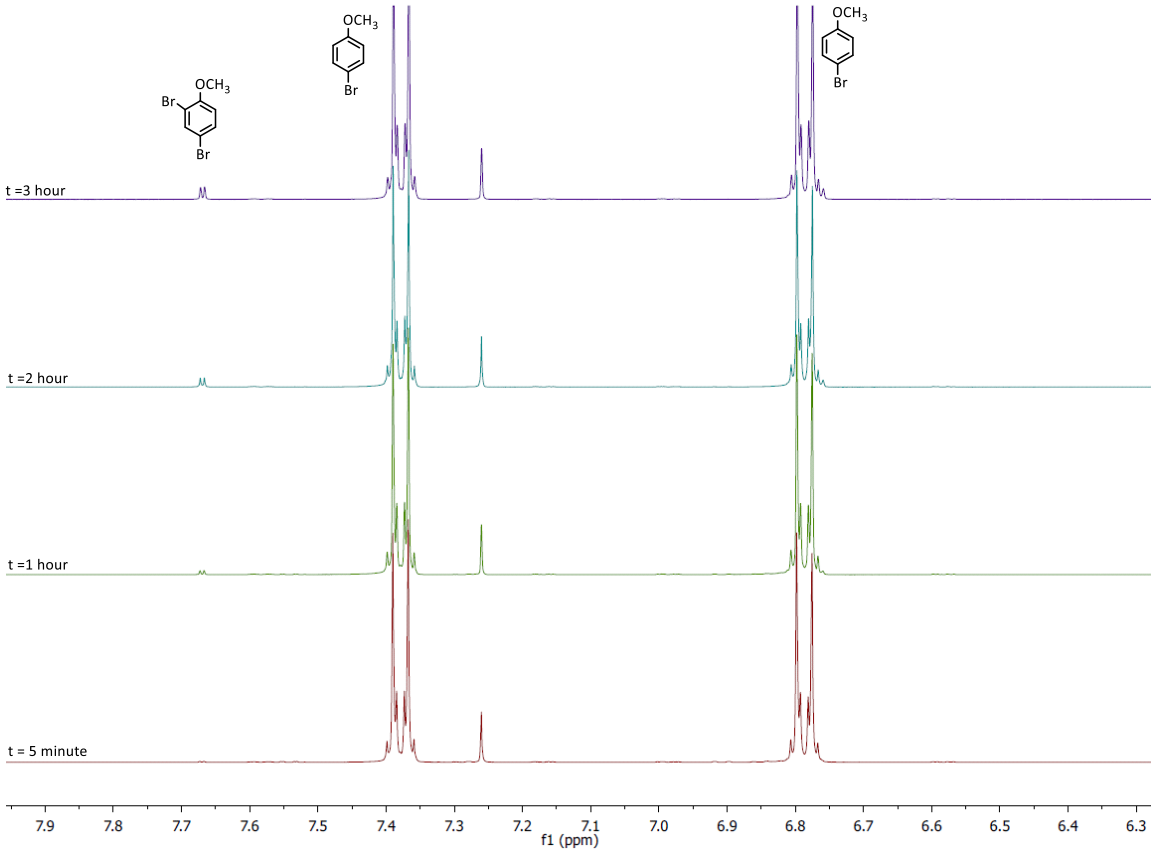

Figure S27: ^{1}H NMR spectrum stack of reaction of anisole and 2 equivalents of Br_2 in $CDCl_3$ over time showing formation of dibromo anisole.

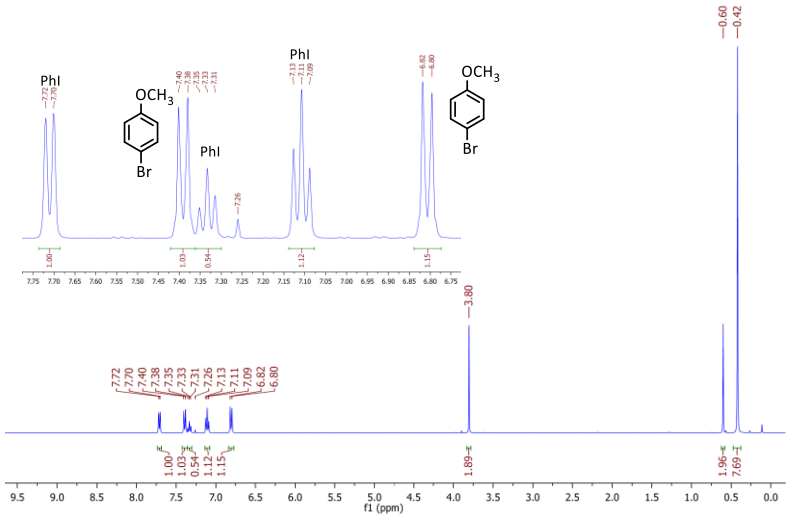

Figure S28: ^{1}H NMR spectrum of reaction of anisole and PIFA/2TMSBr in $CDCl_3$ (inset) aryl region of spectrum with peaks labelled to corresponding compound.

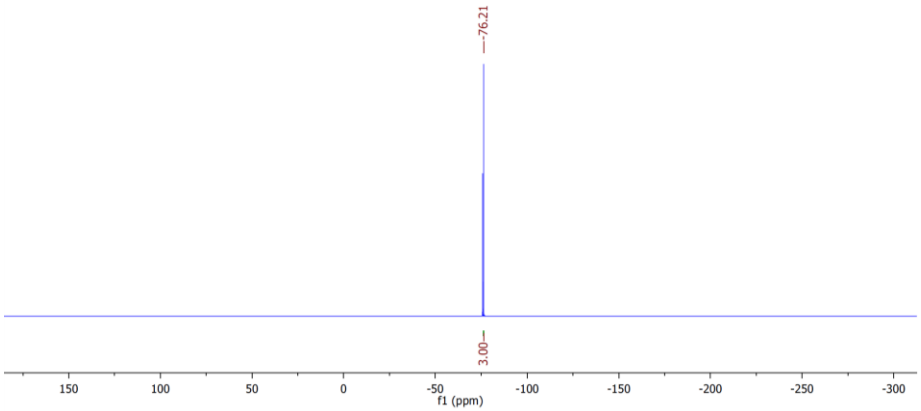

Figure S29: ^{19}F NMR spectrum of reaction of anisole and PIFA/2TMSBr in $CDCl_3$.

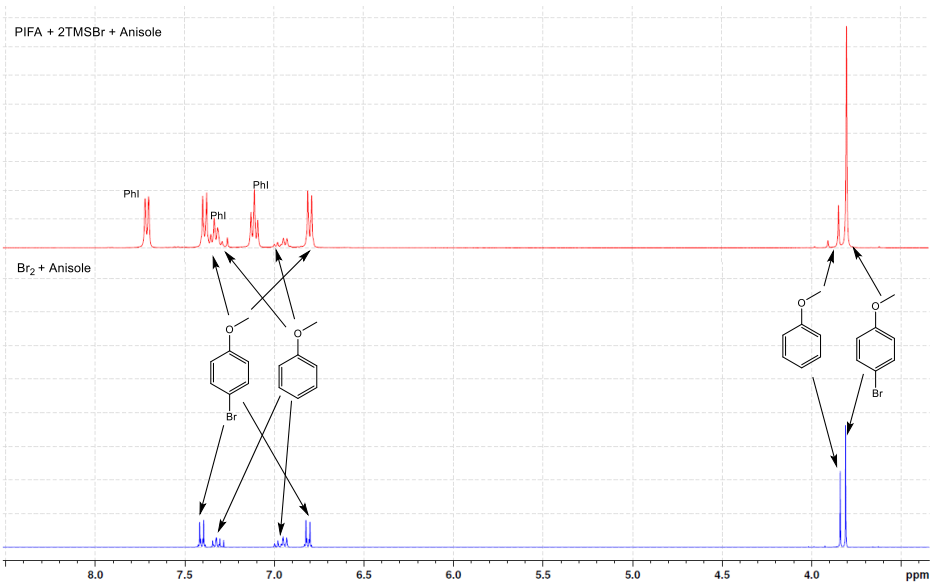

Figure S30: Stacked *in situ* ^{1}H NMR spectra after 5 minutes of PIFA/2TMSBr (red) and Br_2 (blue) with anisole in $CDCl_3$.

g. Bromination of 1,3,5-trimethoxy benzene

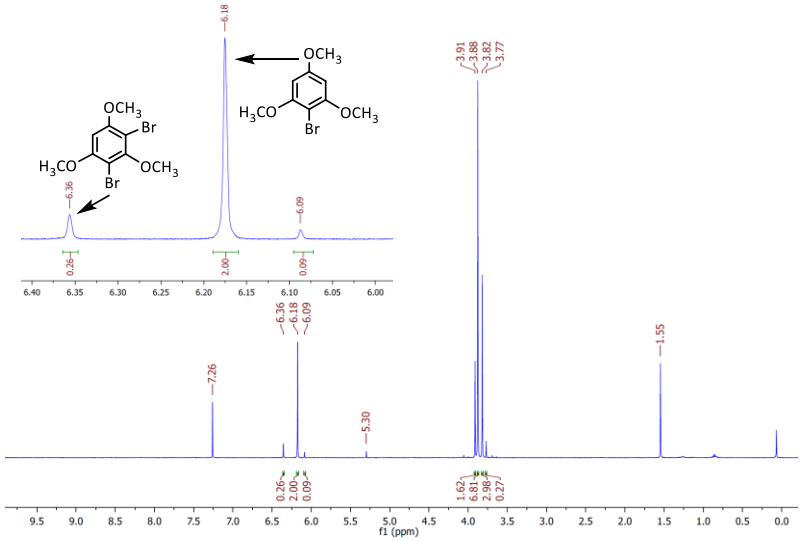

Figure S31: ^{1}H NMR spectrum of reaction of 1,3,5-trimethoxy benzene and Br_2 under N_2 in $CDCl_3$ (inset) aryl region of spectrum with peaks labelled to corresponding compound.

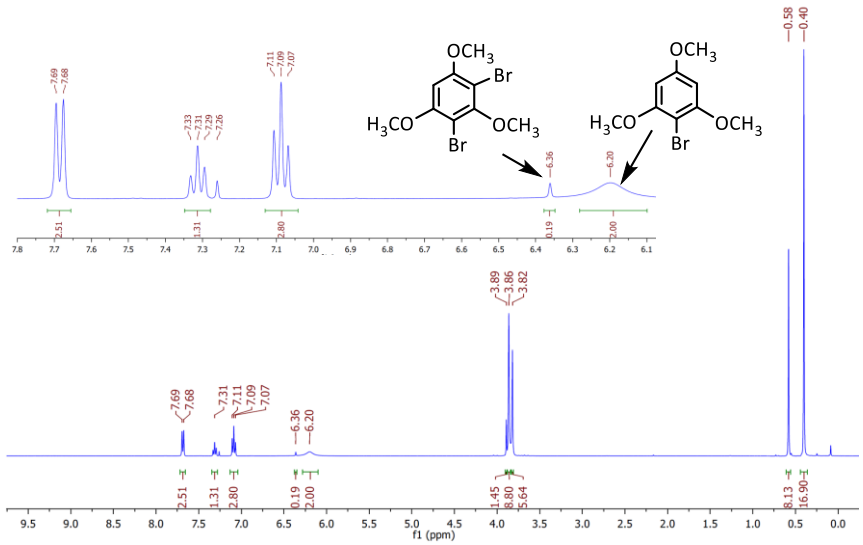

Figure S32: ^{1}H NMR spectrum of reaction of 1,3,5-trimethoxy benzene and PIFA/2TMSBr in $CDCl_3$ (inset) aryl region of spectrum with peaks labelled to corresponding compound.

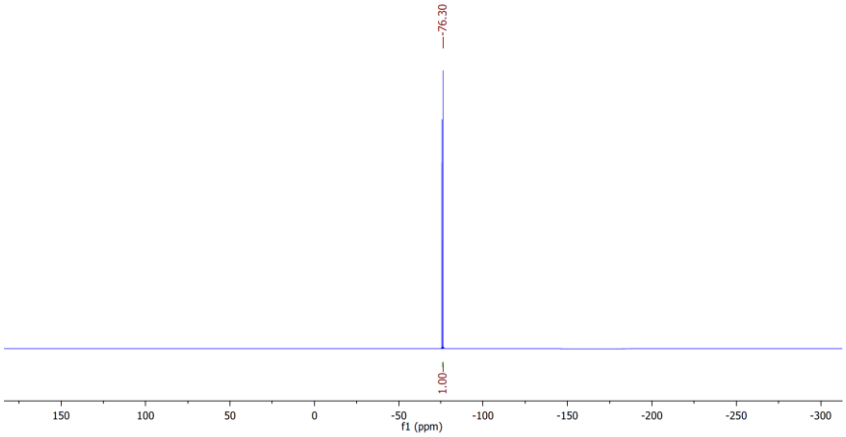

Figure S33: ^{19}F NMR spectrum of reaction of 1,3,5-trimethoxy benzene and PIFA/2TMSBr in $CDCl_3$.

h. Bromination of Salicylic acid

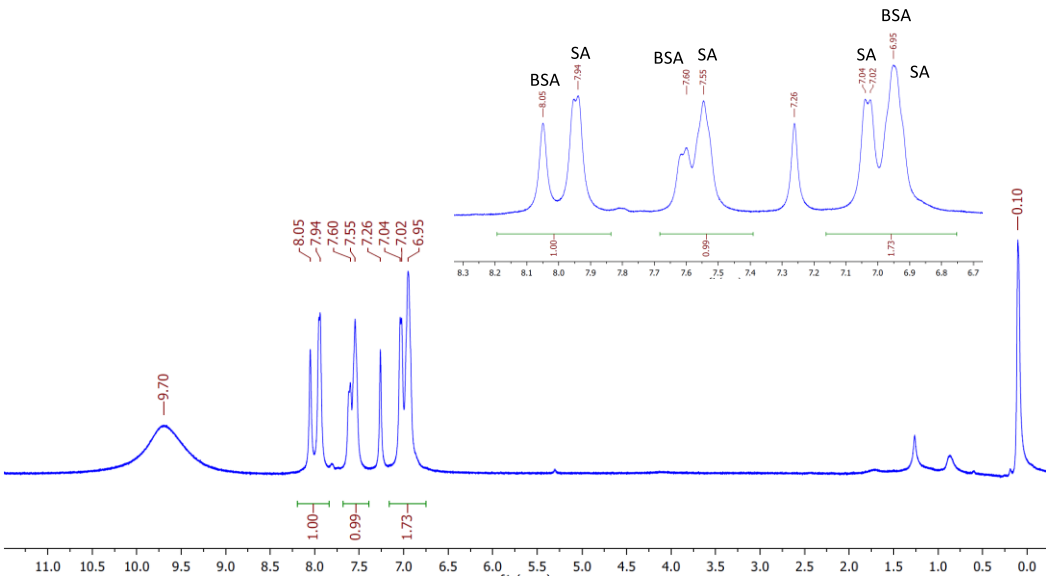

Figure S34: ^{1}H NMR spectrum of reaction of salicylic acid and Br_2 under N_2 in $CDCl_3$ (inset) aryl region of spectrum with peaks labelled to corresponding compound where SA = salicylic acid and BSA = bromo salicylic acid.

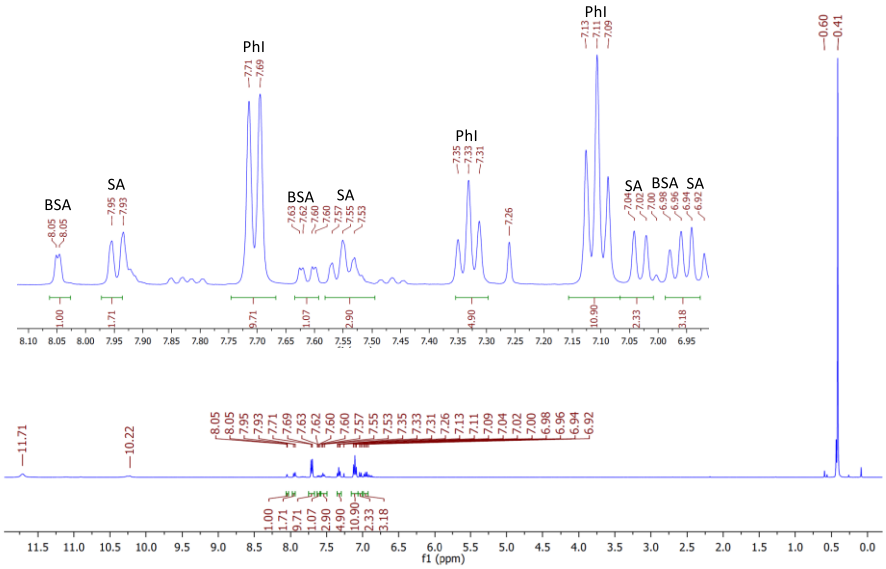

Figure S35: ^{1}H NMR spectrum of reaction of salicylic acid and PIFA/2TMSBr in $CDCl_3$ (inset) aryl region of spectrum with peaks labelled to corresponding compound where SA = salicylic acid and BSA = bromo salicylic acid.

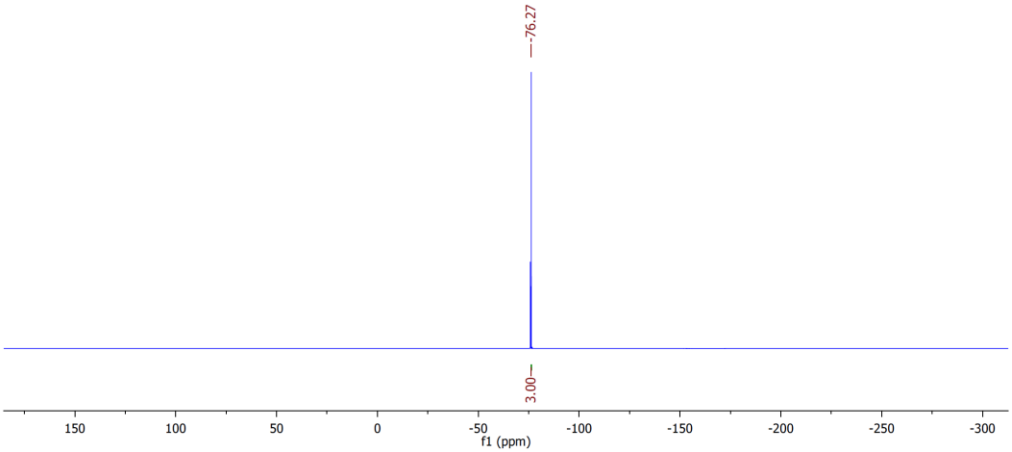

Figure S36: ^{19}F NMR spectrum of reaction of salicylic acid and PIFA/2TMSBr in $CDCl_3$.

i. Bromination of 1,4-dimethoxy benzene

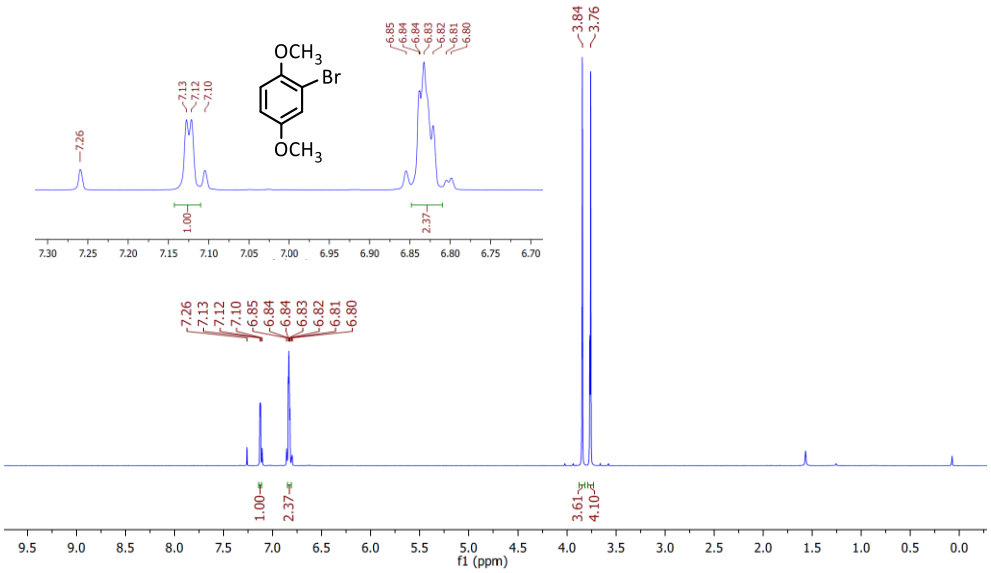

Figure S37: ^{1}H NMR spectrum of reaction of 1,4-dimethoxy benzene and Br_2 under N_2 in $CDCl_3$ (inset) aryl region of spectrum with peaks labelled to corresponding compound.

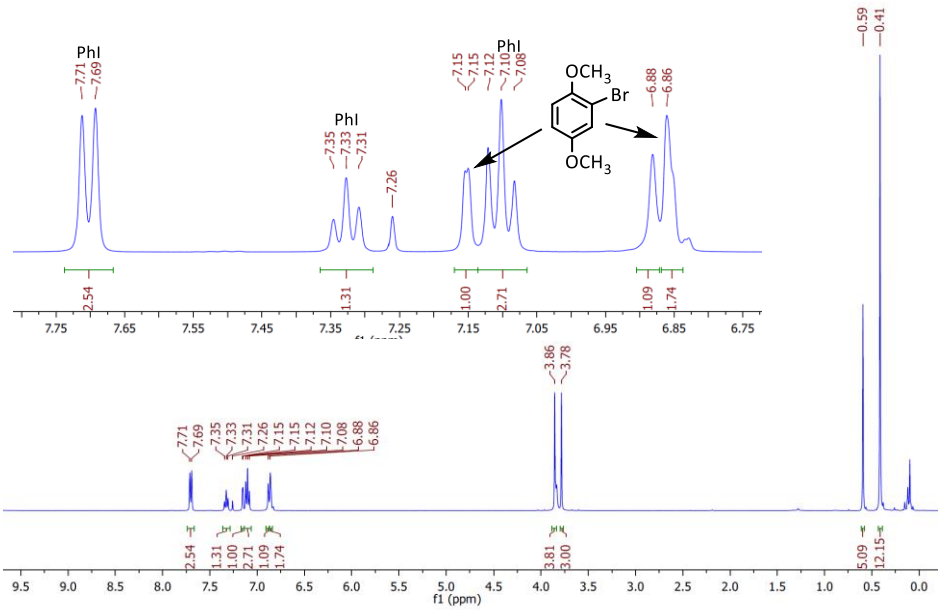

Figure S38: ^{1}H NMR spectrum of reaction of 1,4-dimethoxy benzene and PIFA/2TMSBr in $CDCl_3$ (inset) aryl region of spectrum with peaks labelled to corresponding compound.

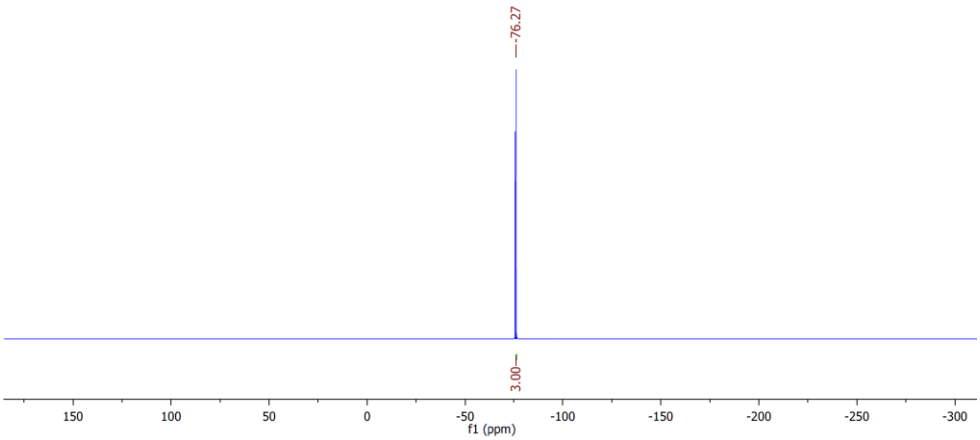

Figure S39: ^{19}F NMR spectrum of reaction of 1,4-dimethoxy benzene and PIFA/2TMSBr in $CDCl_3$.

j. Bromination of Mesitylene

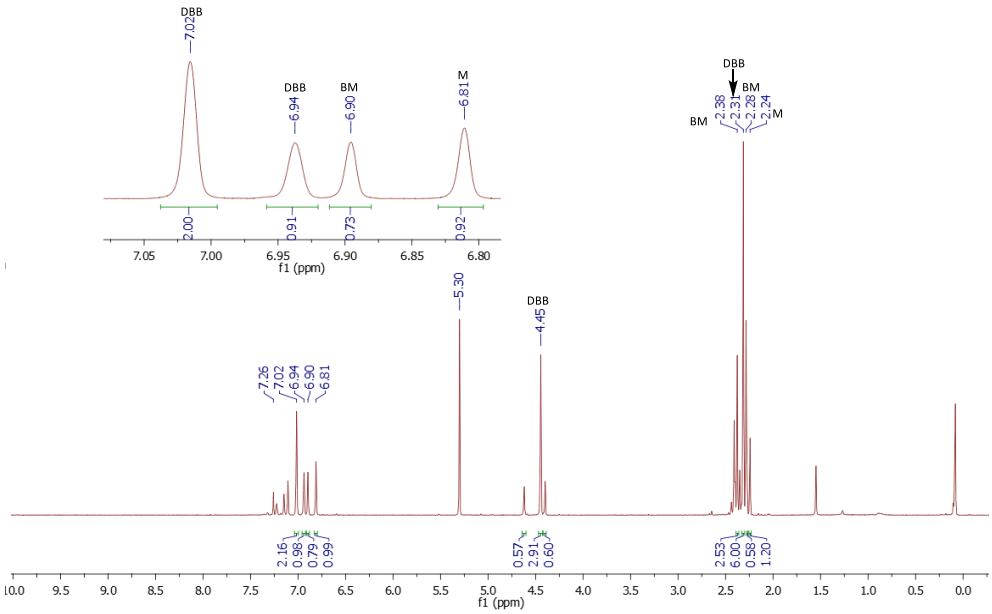

Figure S40: ^{1}H NMR spectrum of reaction of mesitylene and Br_2 under N_2 in $CDCl_3$ (inset) aryl region of spectrum with peaks labelled to corresponding compound where M = mesitylene, BM= bromo mesitylene and DBB= 3,5-dimethylbenzyl bromide.

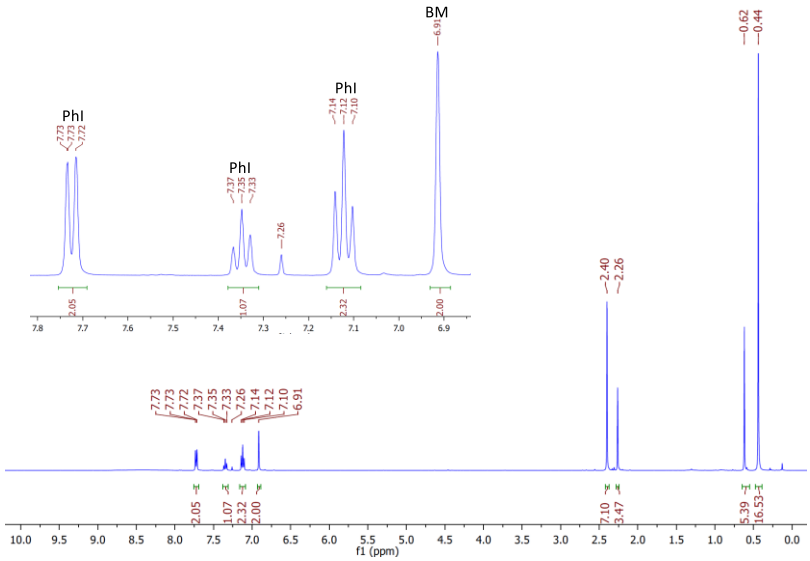

Figure S41: ^{1}H NMR spectrum of reaction of mesitylene and PIFA/2TMSBr in $CDCl_3$ (inset) aryl region of spectrum with peaks labelled to corresponding compound where BM= bromo mesitylene.

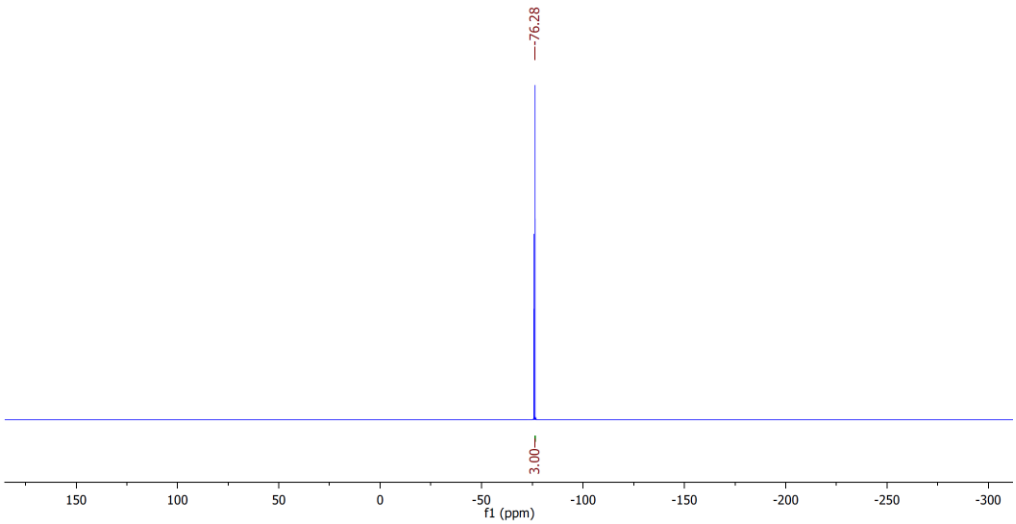

Figure S42: ^{19}F NMR spectrum of reaction of mesitylene and PIFA/2TMSBr in $CDCl_3$.

k. PIDA + 2 NaBr

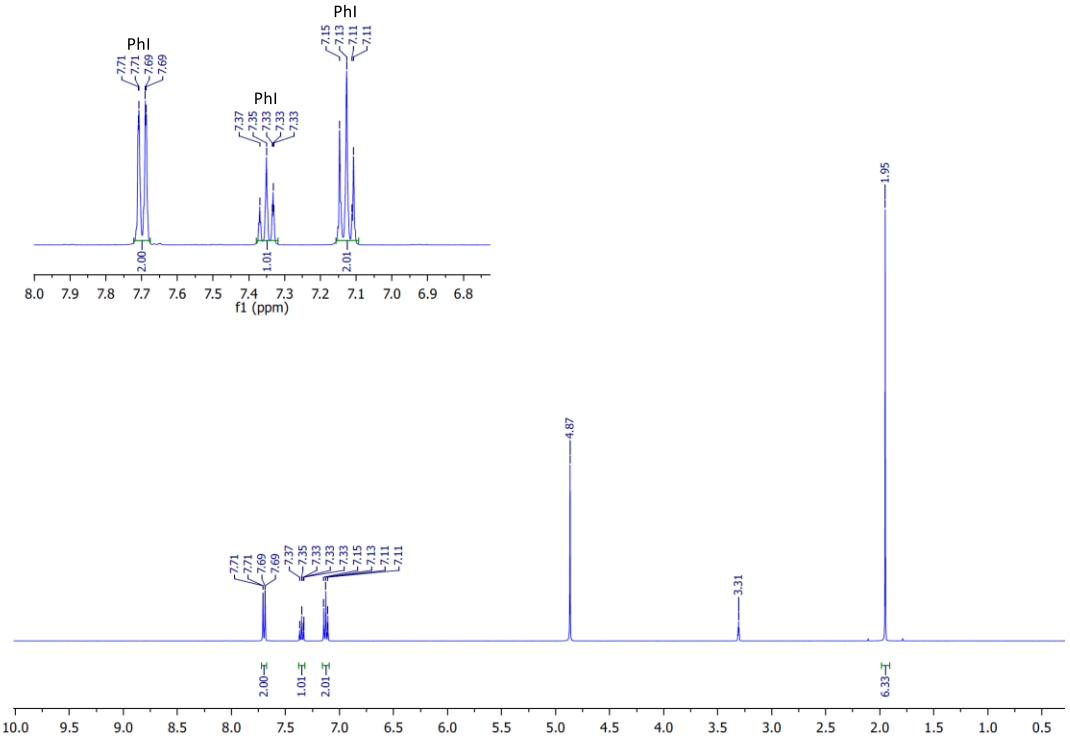

Figure S43: ^{1}H NMR spectrum of reaction of PIDA/2NaBr in MeOD (inset) aryl region of spectrum with peaks labelled to corresponding compound.

l. PIDA + 2 NaBr + Benzaldehyde

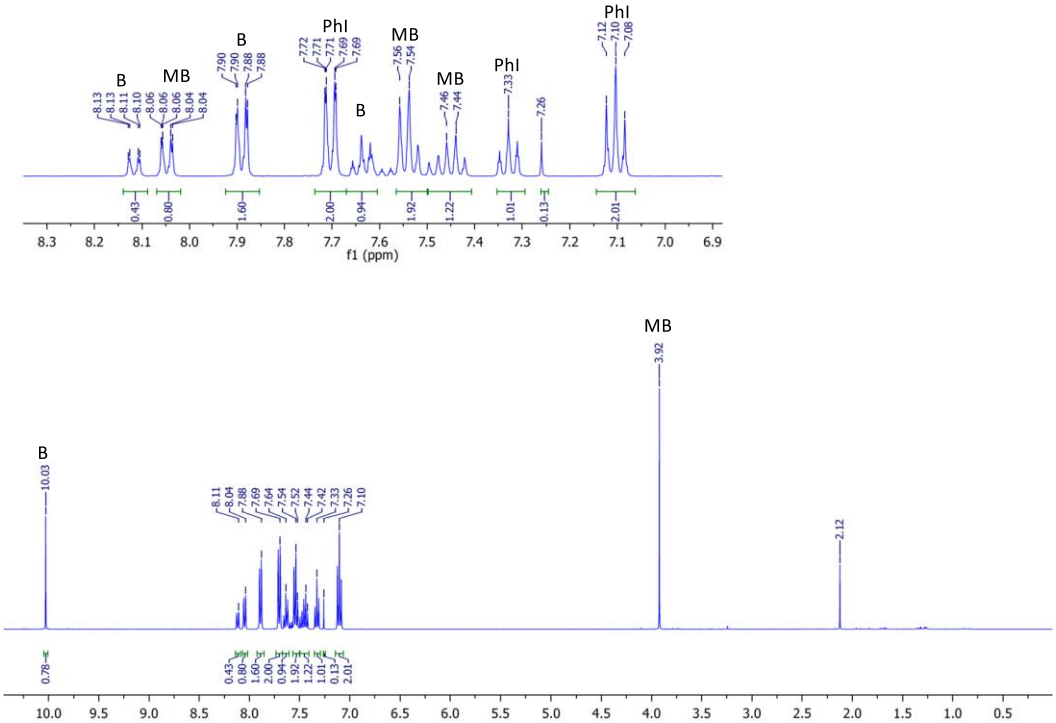

Figure S44: ^{1}H NMR spectrum of reaction of PIDA/2NaBr and benzaldehyde in MeOD (inset) aryl region of spectrum with peaks labelled to corresponding compound where B = benzaldehyde and MB = Methyl benzoate.

m. Br_2 + Benzaldehyde

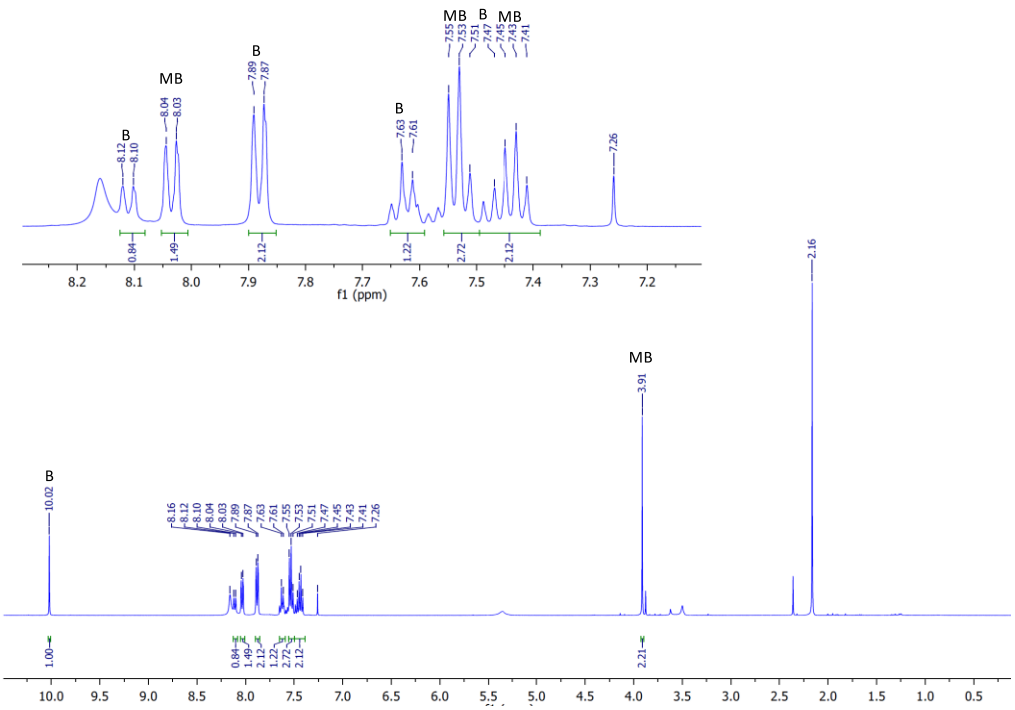

Figure S45: ^{1}H NMR spectrum of reaction of Br_2 and benzaldehyde in MeOD (inset) aryl region of spectrum with peaks labelled to corresponding compound where B = benzaldehyde and MB = Methyl benzoate.

n. PIDA + $[NBu_4][Br]$

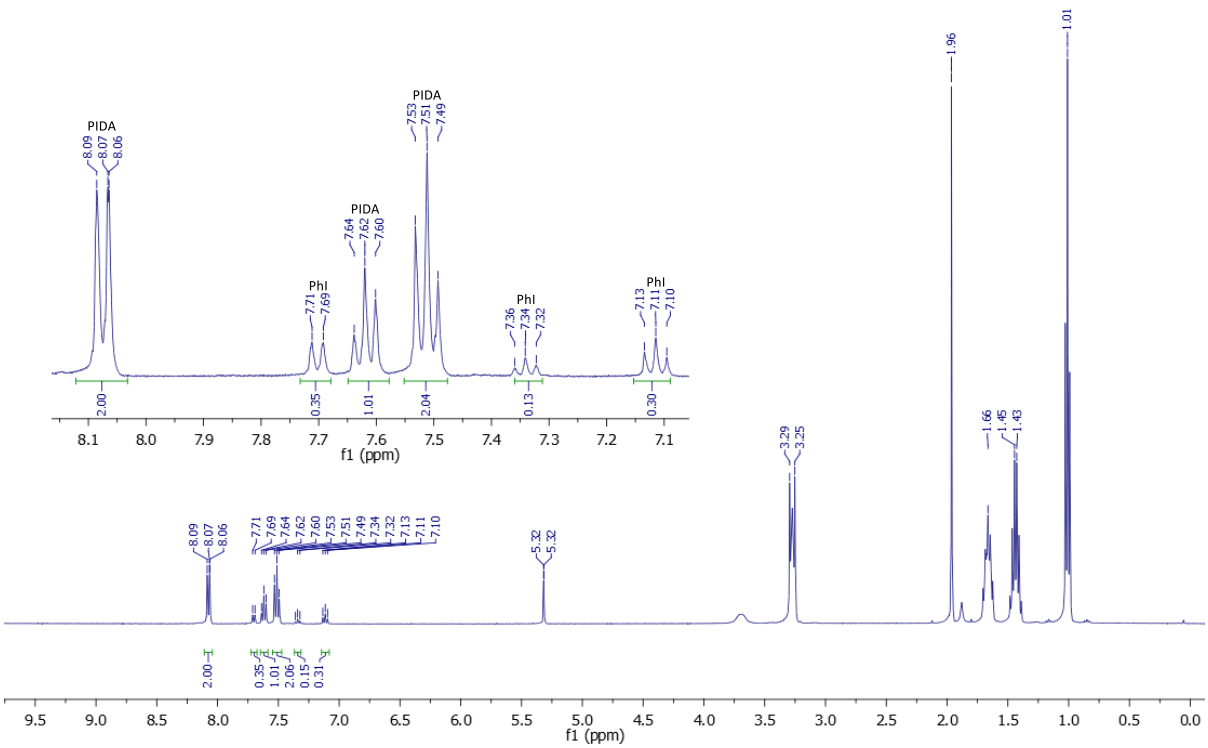

Figure S46: ^{1}H NMR spectrum of reaction of PIDA and $[NBu_4][Br]$ in CD_2Cl_2 (inset) aryl region of spectrum with peaks labelled to corresponding compound.

o. PIDA + 2 [NBu_4][Br]

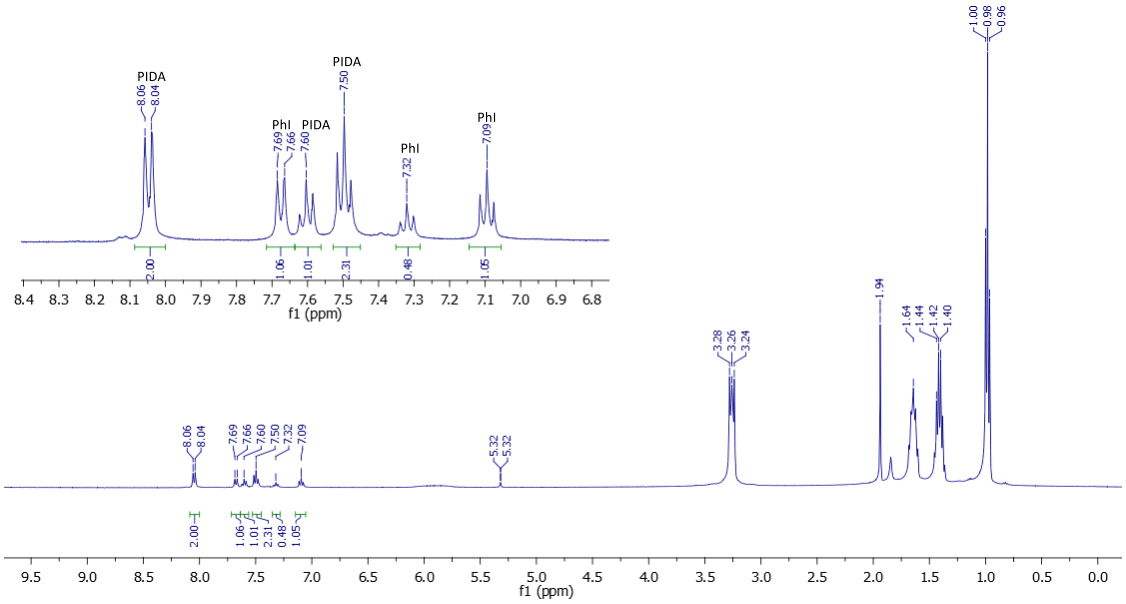

Figure S47: ^{1}H NMR spectrum of reaction of PIDA and 2 equivalents of[NBu_4][Br] in CD_2Cl_2 (inset) aryl region of spectrum with peaks labelled to corresponding compound.

1.4 UV-Vis Investigations

a. Br_2

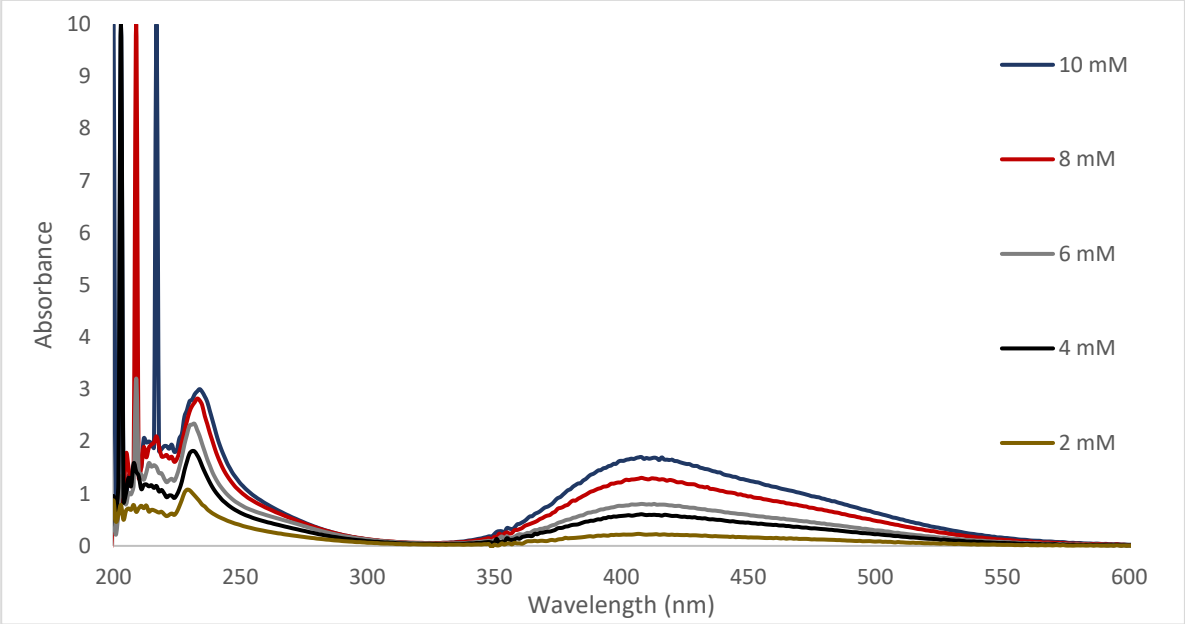

Figure S48: Absorbance vs. wavelength plot for various dilutions of Br_2 in CH_2Cl_2.

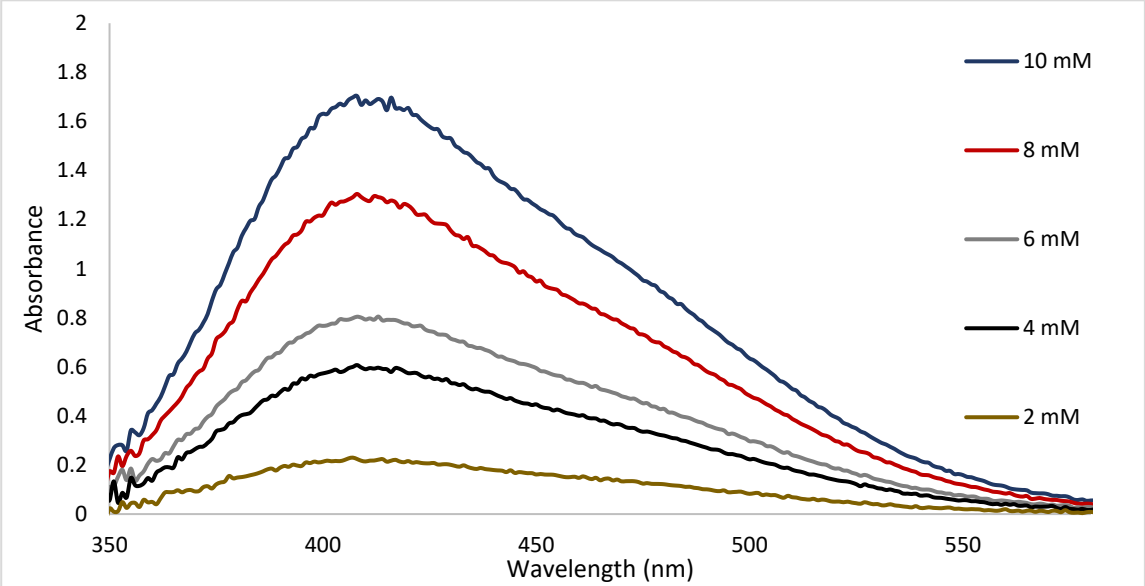

Figure S49: Absorbance at λ_{max} for different dilutions of Br_2 in CH_2Cl_2.

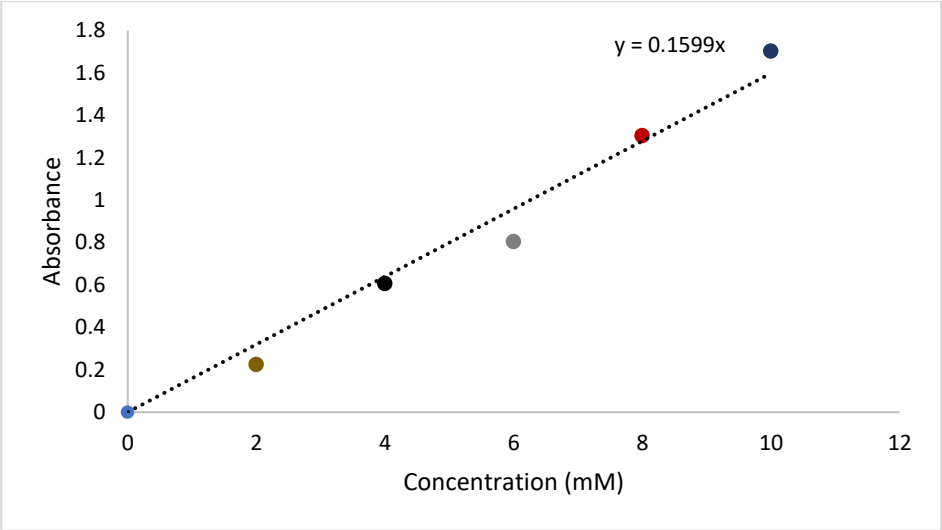

Figure S50: Absorbance for different dilutions of Br_2 in CH_2Cl_2 at λ_{max} wavelength.

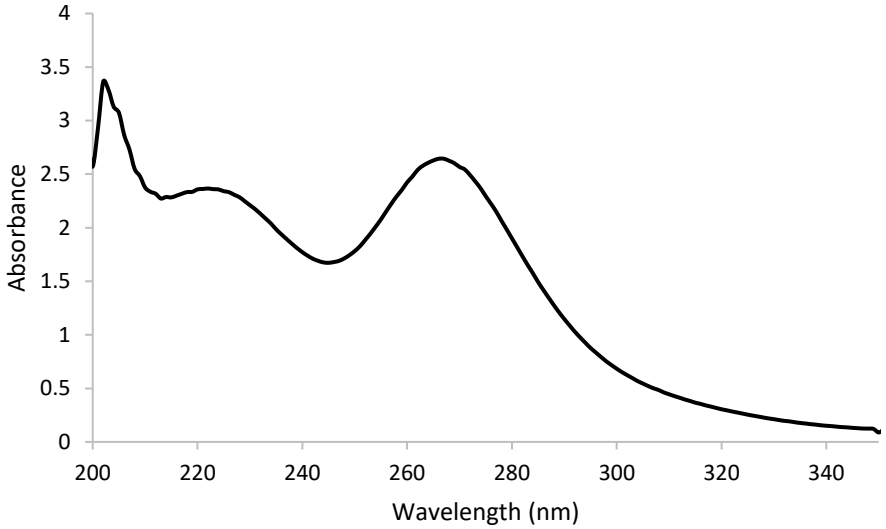

Figure S51: Absorbance vs. wavelength plot for 4 mM Br_2 in MeOH.

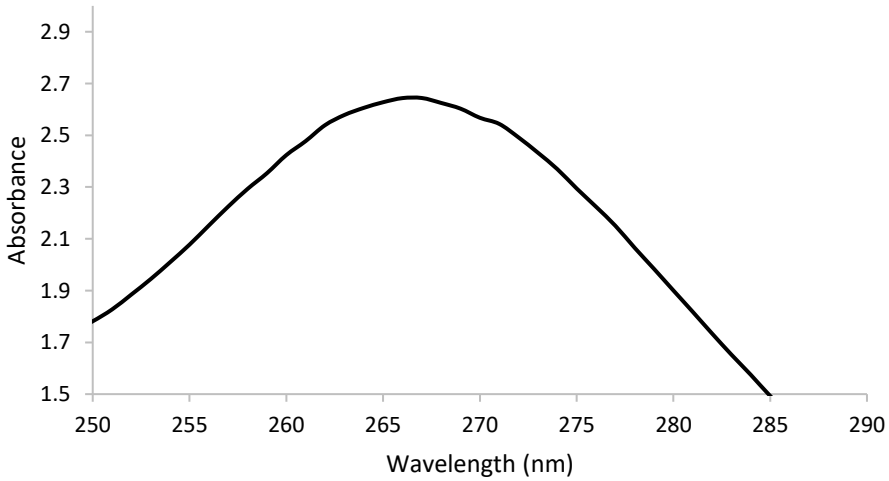

Figure S52: λ_{max} wavelength for 4 mM Br_2 in MeOH.

b. PhI + Br_2

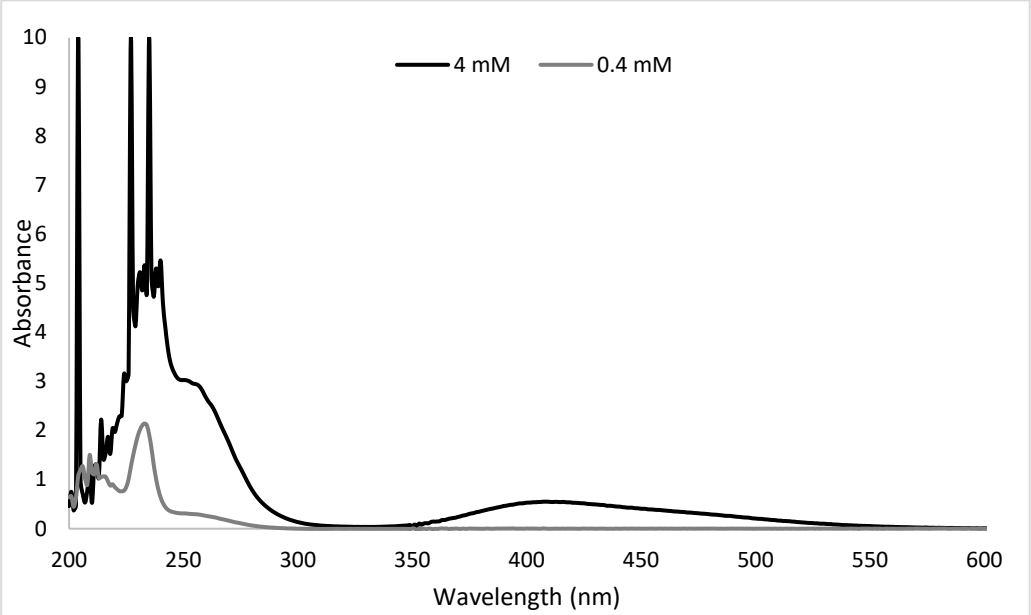

Figure S53: Absorbance vs. wavelength (nm) plot for Br_2 and PhI in CH_2Cl_2.

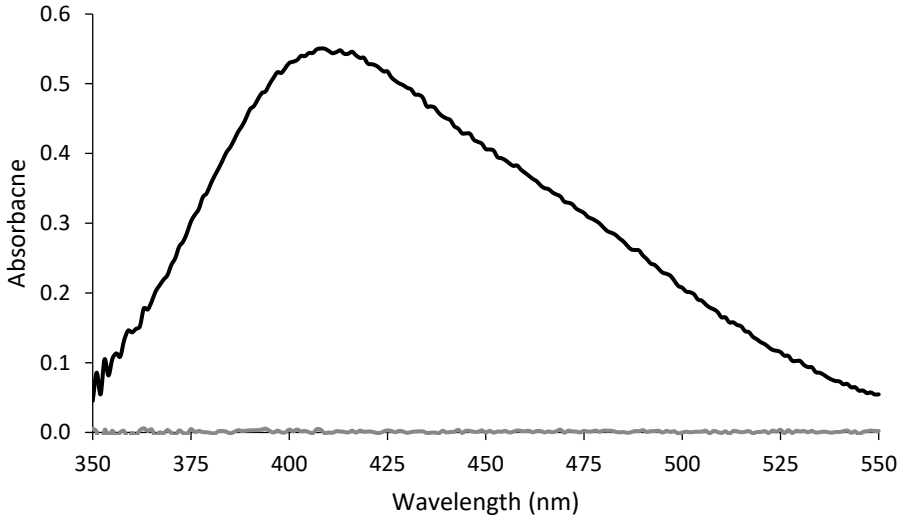

Figure S54: λ_{max} wavelength for 4 mM Br_2 and PhI in CH_2Cl_2.

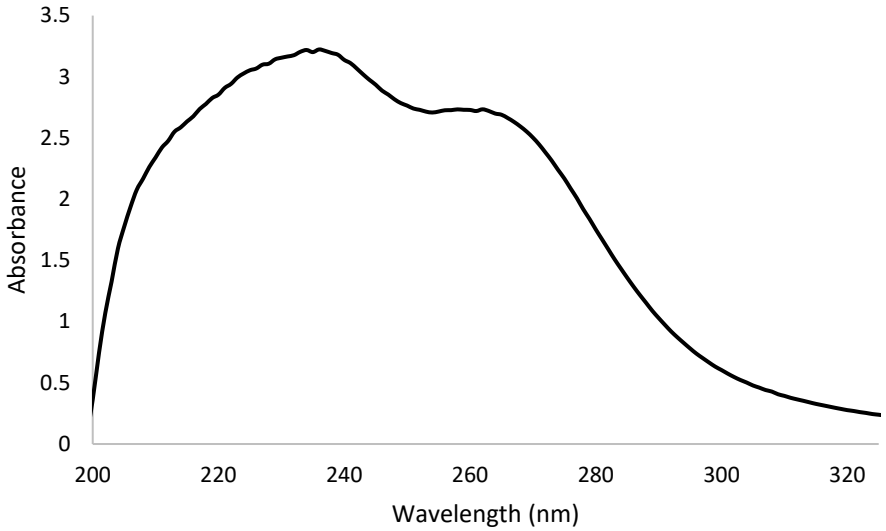

Figure S55: Absorbance vs. wavelength (nm) plot for 4 mM Br_2 and PhI in MeOH.

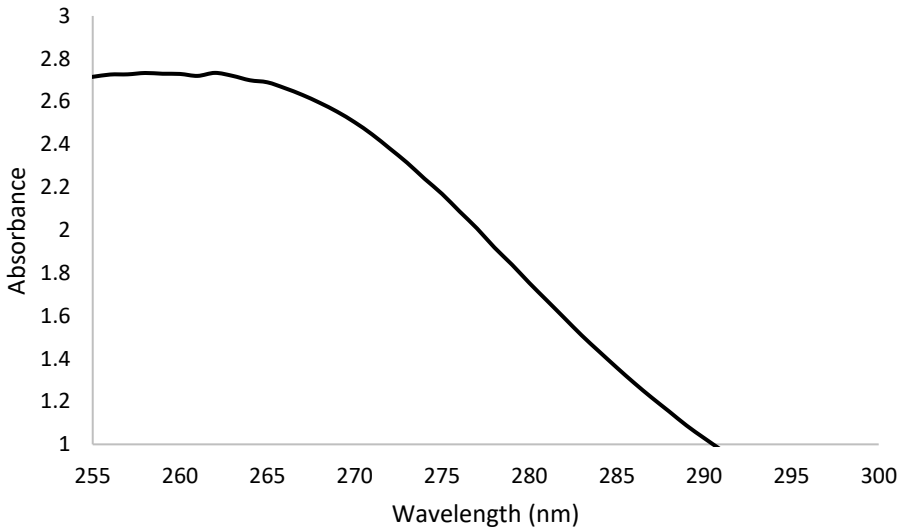

Figure S56: λ_{max} wavelength for 4 mM Br_2 and PhI in MeOH.

c. PIFA + TMSBr

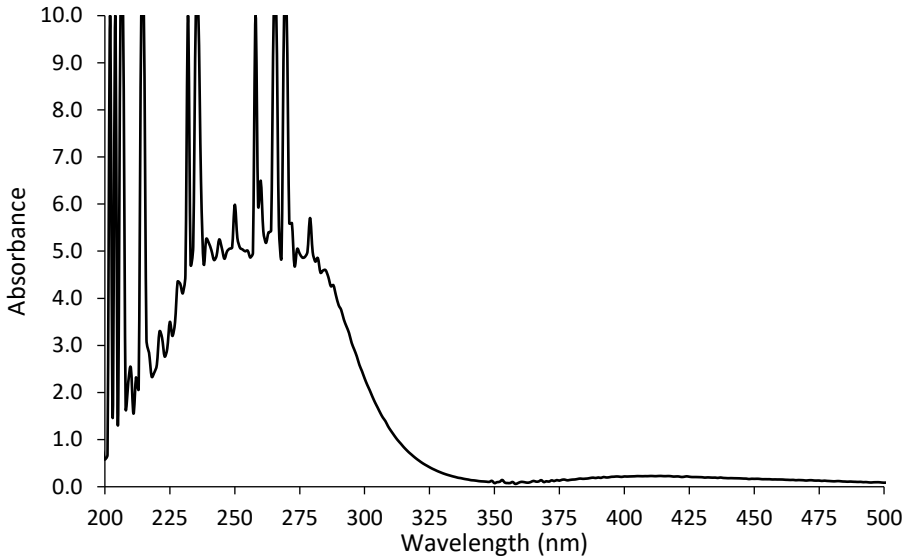

Figure S57: Absorbance vs. wavelength (nm) plot for 4 mM PIFA and 1 equivalent of TMSBr in CH_2Cl_2.

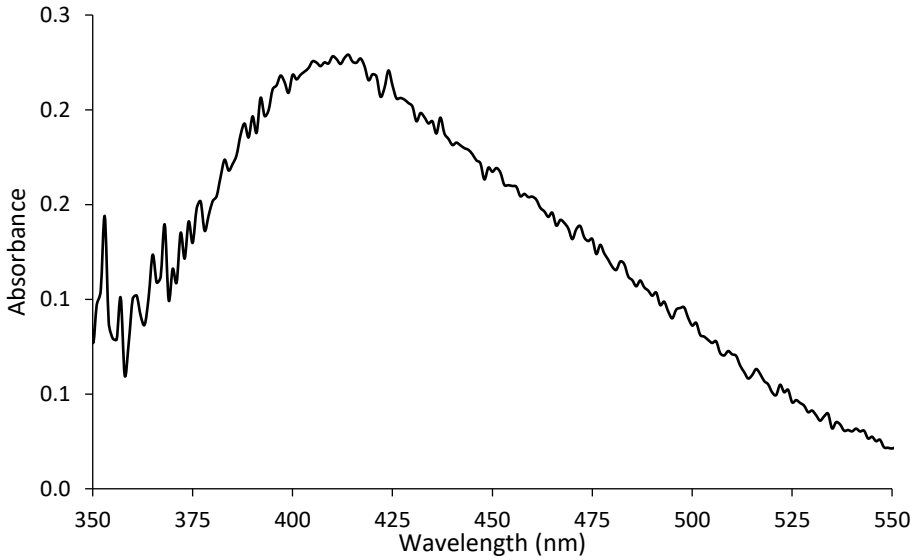

Figure S58: λ_{max} wavelength for 4 mM PIFA and 1 equivalent of TMSBr in CH_2Cl_2.

d. PIFA + 2 TMSBr

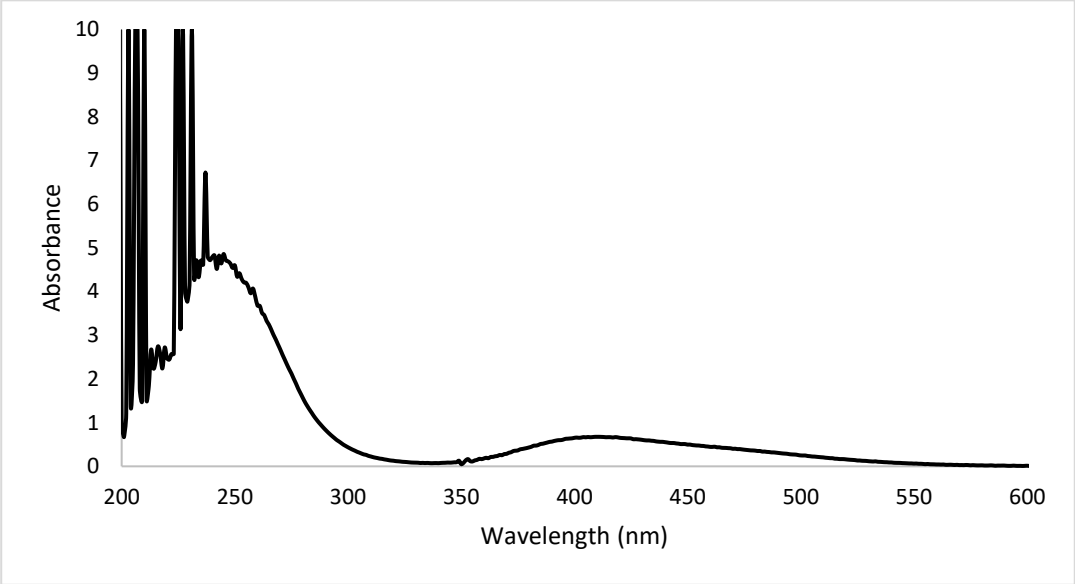

Figure S59: Absorbance vs. wavelength (nm) plot for 4 mM PIFA and 2 equivalents of TMSBr in CH_2Cl_2.

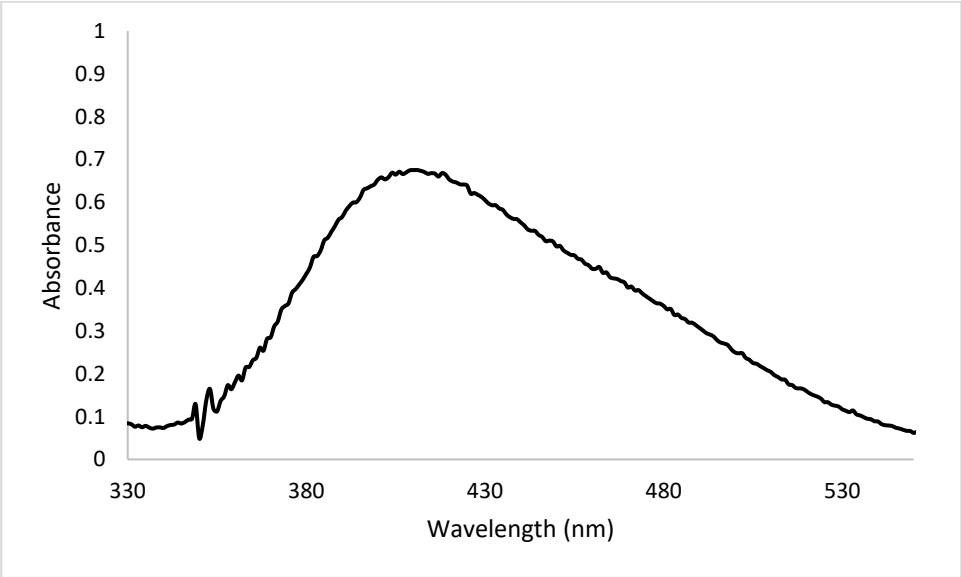

Figure S60: λ_{max} wavelength for 4 mM PIFA and 2 equivalents of TMSBr in CH_2Cl_2.

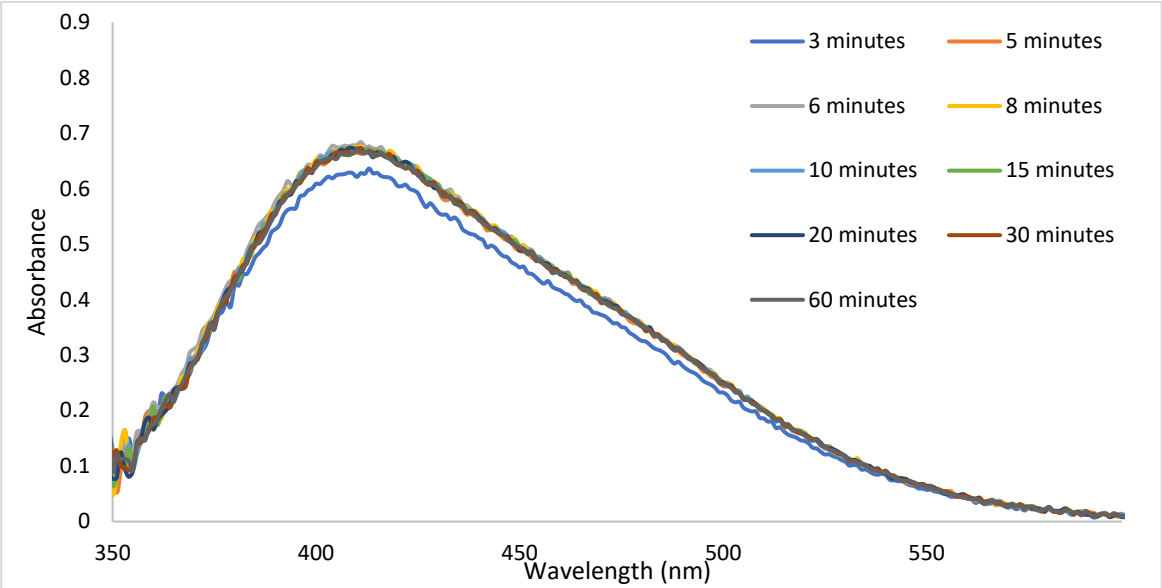

Figure S61: λ_{max} wavelength for 4 mM solution of PIFA and 2 equivalents of TMSBr in CH_2Cl_2 over time.

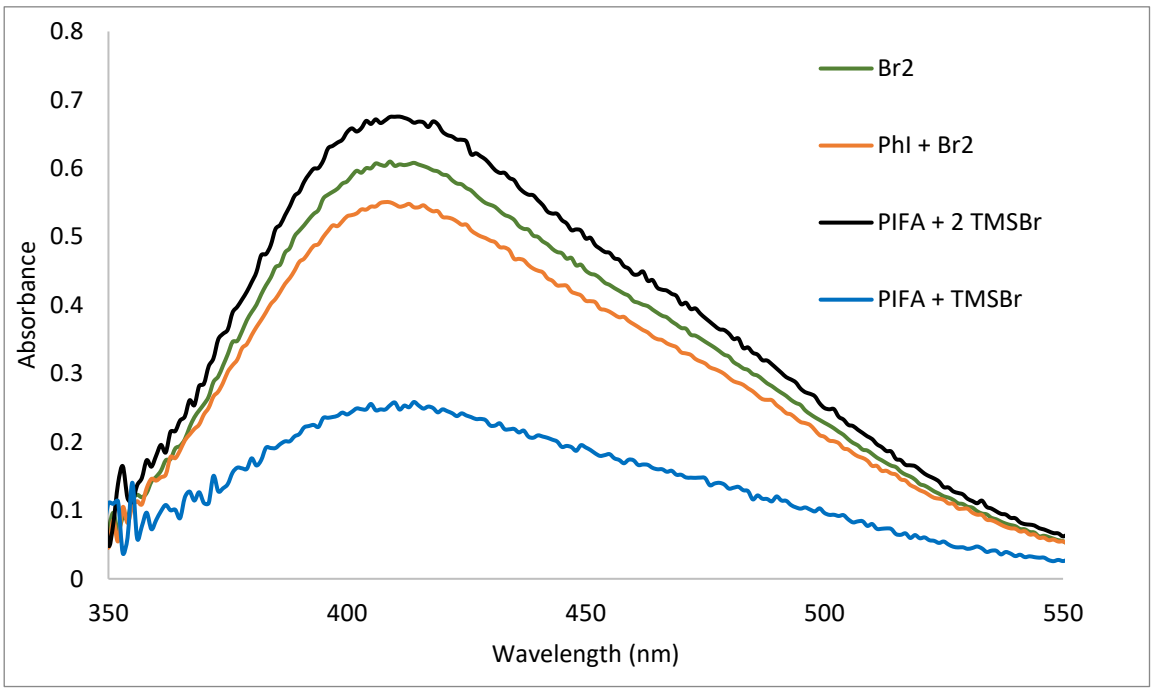

Figure S62: λ_{max} for 4 mM solutions of Br_2, PhI + Br_2, PIFA + TMSBr, and PIFA and 2 equivalents of TMSBr in CH_2Cl_2.

e. PIDA + 2 NaBr

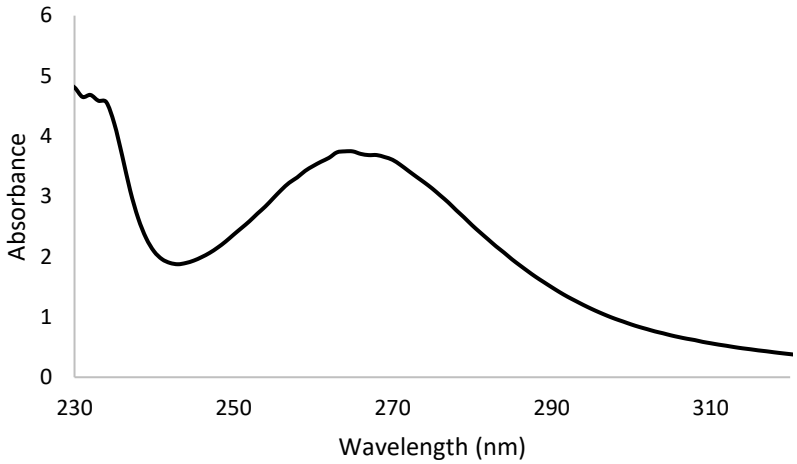

Figure S63: Absorbance vs. wavelength (nm) plot for 0.04 M PIDA and 2 equivalents of NaBr in MeOH.

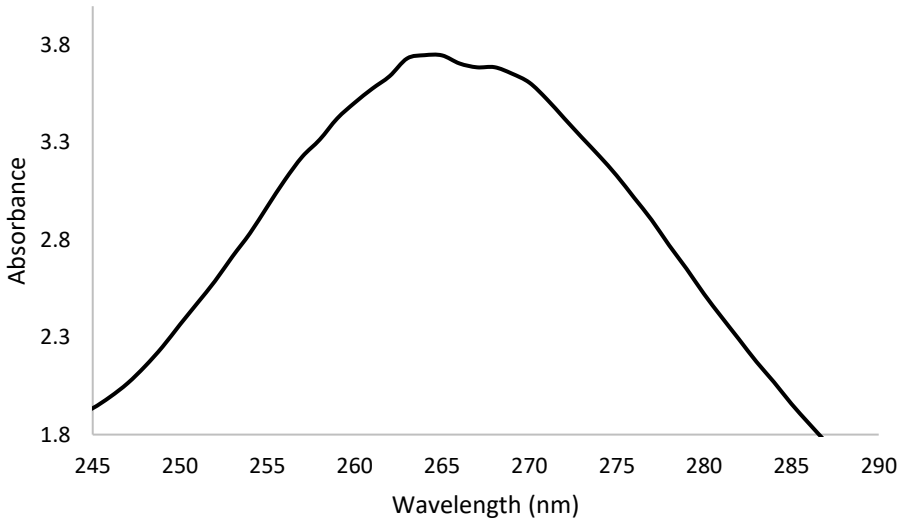

Figure S64: λ_{max} wavelength for 0.04 M PIDA and 2 equivalents of NaBr in MeOH.

1.5 ESI-MS Investigations

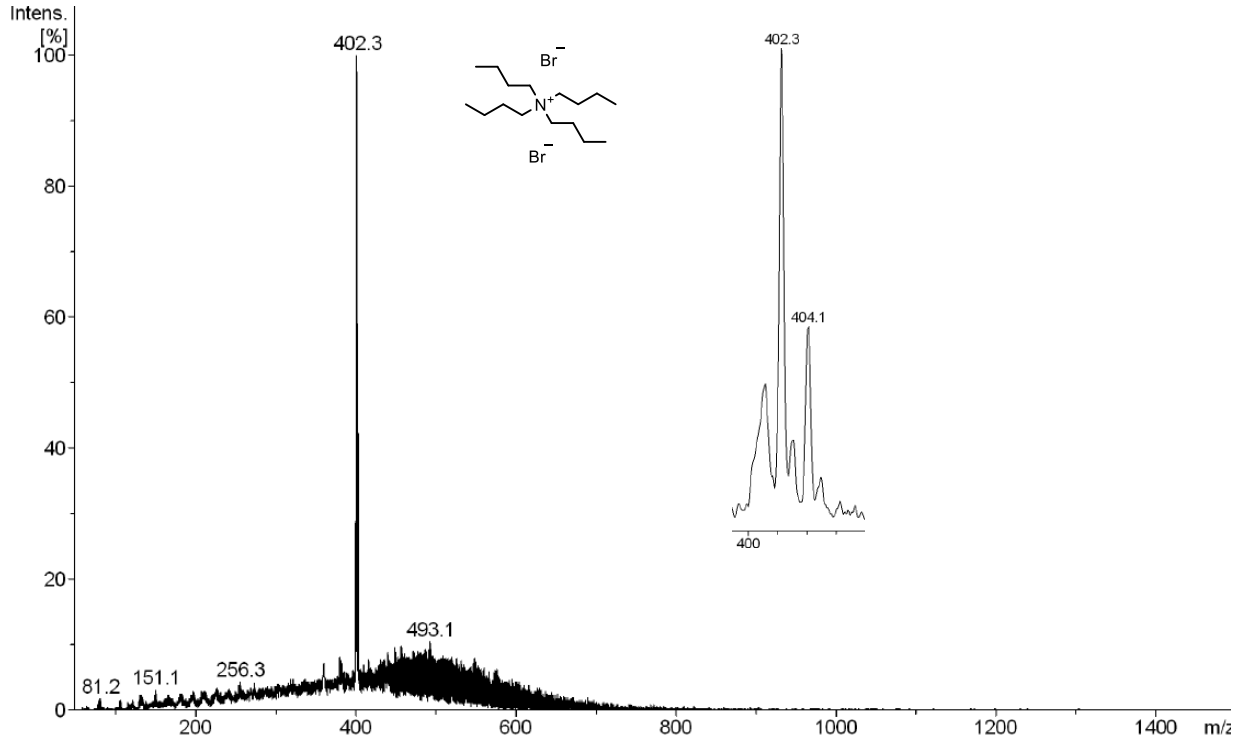

Figure S65: ESI-MS (negative polarity) of PIDA + $[NBu_4][Br]$ in CH_2Cl_2 and species responsible for major signal (inset) isotope pattern for major signal.

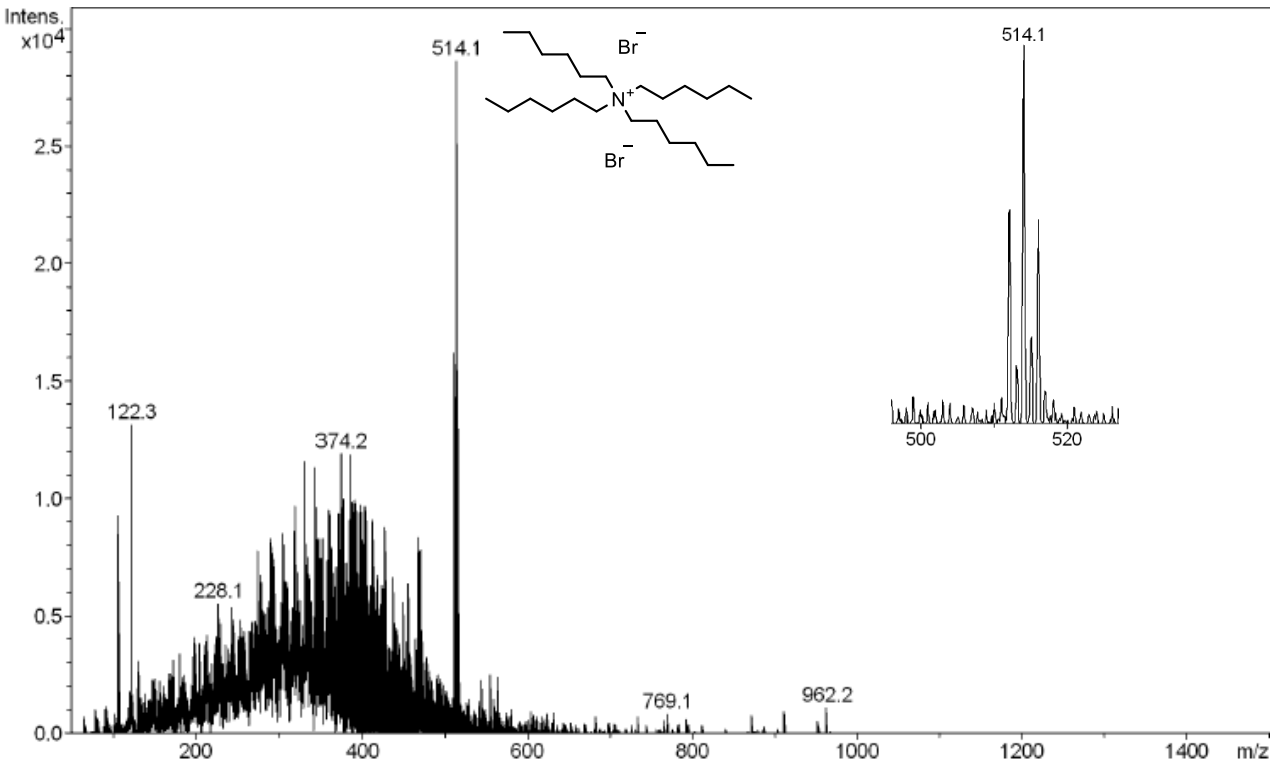

Figure S66: ESI-MS (negative polarity) of PIDA + $[NHex_4][Br]$ in CH_2Cl_2 and species responsible for major signal (inset) isotope pattern for major signal.

Computational Section

2.1 Computational Details

Geometry optimizations with ωB97X-D3(BJ) were carried out in Orca 5.0.3.[9] The def2-SVP and def2-TZVP basis sets[10] (and associated ECP for iodine)[10, 11] were used in addition to the resolution of identity approximations (RIJCOSX) for both Coulomb and Hartree-Fock exchange integrals with the def2/J[12] and def2/C[13] auxiliary basis sets. A tight SCF convergence criterion (±1.0E-08 au) was employed in all calculations. Solvation was included in all calculations utilising the CPCM[14] models with parameters for CH_2Cl_2. Vibrational frequency calculations were carried out analytically at the same level of theory as any geometry optimization calculation. Within Orca, transition state optimizations employed default algorithms (optts keyword) or the NEB-TS approach.[15] Intrinsic reaction coordinate (IRC) calculations were carried out for all optimized transition state structures.

Geometry optimizations with B3LYP-D3, B3LYP-D3(BJ), M06-2X, and ωB97XD were carried out in Gaussian 09 Rev E.01[16] and Gaussian 16 Rec C.01.[17] Default parameters were employed unless specified. Vibration frequency calculations were performed for all optimized stationary points on the potential energy surface to confirm that minima had no imaginary frequencies, while transition states had one imaginary frequency. Intrinsic reaction coordinate (IRC) calculations were carried out within Gaussian 09 using the LQA algorithm with 100 steps. The McGrath and Radom[18] 6-31+G(d) basis set for Br was taken from the internal library in Gaussian. The Rassolov[19] 6-31+G(d) basis for Br was employed by use of the GTBas1 keyword in Gaussian. Solvation was included in all calculations. In Gaussian 09, a polarizable continuum model (PCM) model was utilised, while in Gaussian 16 a PCM model was employed together with Truhlar's SMD model. In all instances a solvent of dichloromethane (CH_2Cl_2) was utilised.

Single-point energy calculations were carried out within Orca 5.0.3[9] with a range of DFT functionals (PW6B95-D3(BJ), B97M-D4, ωB97X-D3(BJ), ωB97M-D3(BJ), ωB97M-V, B97M-D4) and DLPNO-CCSD(T)[20, 21], DLPNO-MP2[22, 23] and RI-SCS-MP2,[24] which utilised the SMD[25] solvation model.

2.2 Formation of $PhIBr_2$ from PhI + Br_2

The results of various methods and basis sets are presented in Table S1 to assess basis set and electronic structure method dependence. All methods indicate that formation of $PhIBr_2$ from PhI and Br_2 is endergonic. Calculated ΔG_{corr} is consistently 37-47 kJ/mol; using any of these values would still lead to all single-point energy calculations being endergonic.

Table S1: Calculated ΔG of PhI + Br_2 → $PhIBr_2$. Units of kJ/mol. Geometry and thermal corrections calculated at the same level of theory unless noted.[a]

Method	Basis Sets			ΔE	ΔG	ΔG_{corr}
	C,H	Br	I			
B3LYP-D3 (PCM)	6-31+G(d)	6-31+G(d) internal	LANL2DZ	18.9	58.2	39.3
B3LYP-D3 (PCM)	6-31+G(d)	6-31+G(d) (GTbas1)	LANL2DZ	31.0	70.0	39.0
B3LYP-D3 (PCM)	6-31+G(d)	6-31+G(d) internal	def2-SVP	-26.7	14.0	40.7
B3LYP-D3 (PCM)	6-31+G(d)	6-31+G(d) (GTbas1)	def2-SVP	-17.7	24.3	42.0
B3LYP-D3 (PCM)	6-31+G(d)	def2-SVP	def2-SVP	-18.7	18.3	37.0
B3LYP-D3 (PCM)	def2-SVP	def2-SVP	def2-SVP	-8.8	31.0	39.8
M06-2X (PCM,SMD)	def2-TZVP	def2-TZVP	def2-TZVP	-5.5	36.3	41.8
ωB97XD (PCM,SMD)	def2-TZVP	def2-TZVP	def2-TZVP	-6.9	38.9	45.8
ωB97X-D3(BJ) (CPCM)	def2-SVP	def2-SVP	def2-SVP	-16.7	29.2	45.9
ωB97X-D3(BJ) (CPCM)	def2-TZVP	def2-TZVP	def2-TZVP	-25.5	21.6	47.1
B3LYP-D3/6-31+G(d),LANL2DZ (PCM,CH_2Cl_2) geometry [b]						45.8
PW6B95-D3(BJ)	def2-TZVP			-4.6	41.2	
B97M-D4	def2-TZVP			-22.3	24.8	
MP2 [c]	def2-TZVP			-4.6	41.2	
DLPNO-MP2 (CPCM,SMD)	def2-TZVPP			-15.6	30.2	
RI-SCS-MP2 (CPCM,SMD)	def2-TZVPP			-0.1	45.7	
DLPNO-CCSD(T) (CPCM)	def2-TZVPP			4.6	50.3	
DLPNO-CCSD(T) (CPCM,SMD)	def2-TZVPP			2.0	47.8	
ωB97X-D3(BJ)/def2-TZVP (CPCM,CH_2Cl_2) geometry [b]						47.1
ωB97M-D3(BJ) (SMD)	def2-TZVP			5.1	52.2	
ωB97M-V (SMD)	def2-TZVP			-1.3	45.8	
B97M-D4 (CPCM)	def2-TZVP			-31.7	15.5	
PW6B95-D3(BJ) (CPCM)	def2-TZVP			-22.3	24.8	
DLPNO-MP2 (CPCM, SMD)	def2-TZVPP			-15.9	31.3	
RI-SCS-MP2 (CPCM, SMD)	def2-TZVPP			1.4	48.5	
DLNO-CCSD(T) (CPCM)	def2-TZVPP			6.7	53.8	
DLNO-CCSD(T) (CPCM, SMD)	def2-TZVPP			4.3	51.4	

[a] PCM solvent model with CH_2Cl_2 solvent unless noted. Pure spherical harmonic d,f functions employed in all calculations. ΔG_{corr} is the free energy correction (ΔG - ΔE).

[b] Tabled ΔG is the sum of the electronic energies and thermal correction (G_{corr}) calculated at the same level of theory as the geometry optimization.

The first four rows in Table S1 with B3LYP-D3 indicate with the McGrath and Radom (internal) and Rassolov 6-31+G(d) basis sets for Br give slightly different results, with the Rassolov basis set yielding ΔG that is about 10 kJ/mol more positive. However, the qualitative conclusions are similar with both predicting an exergonic dissociation reaction. Larger differences arise between the LANL2DZ and def2-SVP basis sets and associated ECPs. Different DFT functionals yield similar results with def2 basis sets. Single-point calculations with DLPNO-CCSD(T) and MP2 variants (MP2, DLPNO-MP2, RI-SCS-MP2) similarly indicate that the formation reaction is endergonic.

2.3 Reproduction of $PhIBr_2$ + anisole mechanism from Cossio and Vallribera.[2]

We were able to reproduce the SI results reported by Cossio and Vallribera[2] using the specified method (B3LYP-D3/6-31+G(d),LANL2DZ(iodine) with PCM,CH_2Cl_2 solvation within Gaussian 09 Rev E.01 for the reaction of PhIBr2 and anisole. The reaction mechanism for two Br_2 reacting with anisole (Figure 3 from Cossio and Vallribera) appears to use an ECP for Br (possibly LANL2DZ).

We reproduced both the geometries and energies reported in the SI by Cossio and Vallribera.[2] Some discrepancies are noted between the geometry parameters provided by Cossio and Vallribera[2] in Figure 1 of their manuscript and from the Cartesian coordinates given in the SI. It is assumed that these differences in geometry parameters are simple transcription errors. This is illustrated in Figure S67, with key bond distance parameters for in initial vdW complex (RC1 from Ref 2 is labelled RC2 in our current work) and the initial transition state (TS1 from Ref 2 is labelled TS2 in the current work) associated with bromination of methoxybenzene (anisole). In Figure S67, the black-coloured values are from Figure 1 (Cossio and Vallribera[2]), red-coloured values from the geometries provided in the SI, and blue-coloured values from our optimized B3LYP-D3(BJ)/def2-SVP (PCM,CH_2Cl_2) calculations.

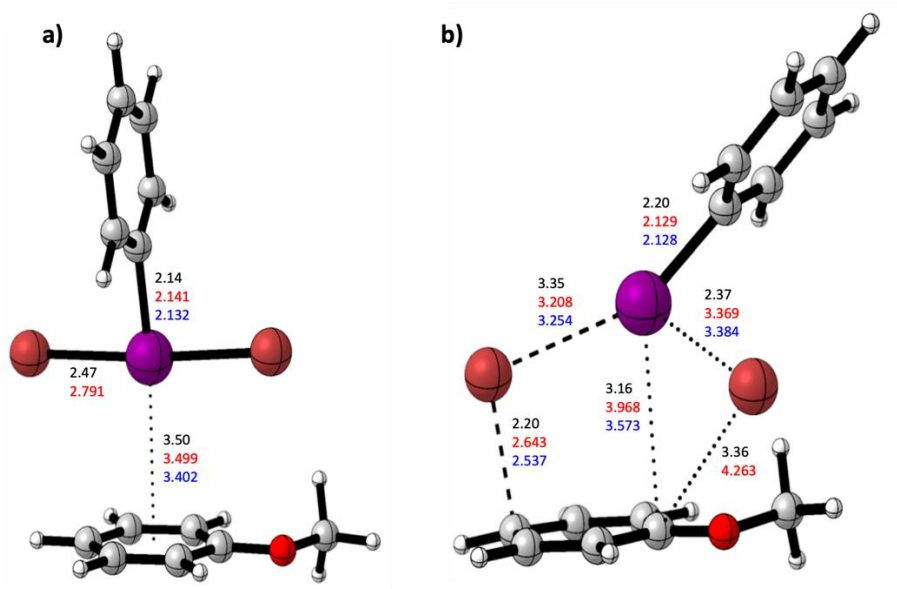

Figure S67. Optimised geometries of (a) RC2 and (b) TS2. Bond distances, black – as reported by Cossio and Vallribera[2] Figure 1, red – obtained from XYZ coordinates provided by Cossio and Vallribera[2] supplementary data, blue – B3LYP-D3(BJ)/def2-SVP (PCM, CH_2Cl_2) optimised geometries.

A number of methods were utilized to explore the reaction mechanism of $PhIBr_2$ and anisole proposed by Cossio and Vallribera[2] (Figure 1 in Ref. 2), with results presented in Table S2. Single-point calculations were carried out with B3LYP-D3, B3LYP-D3(BJ), M06-2X, and wB97XD density functionals at the optimized geometries reported by Cossio and Vallribera[2]. Calculated electronic energies (E_e) were converted to ΔG values by adding the Gibb's free energy correction (ΔG_{corr}) from B3LYP-D3/6-31+G(d),LALN2DZ (PCM,CH_2Cl_2) calculations. Separate geometry optimizations were also carried out with B3LYP-D3, B3LYP-D3(BJ), M06-2X, and wB97XD density functionals.

Table S2: Calculated ΔG of the potential energy surface for the reaction of $PhIBr_2$ and methoxybenzene (anisole). All results given as ΔG relative to PhIBr2 and anisole, in units of kJ/mol.

	Method [a]	RC1	TS1	syn-INT1	anti-INT1	Barrier
1	B3LYP-D3/6-31+G(d),LANL2DZ (PCM,CH_2Cl_2) Ref 2. SI data	25.2	118.2	21.7	16.8	93.0
2	B3LYP-D3/6-31+G(d),LANL2DZ (PCM,CH_2Cl_2) SP G09 (6D)	25.2	118.2	21.7	16.8	93.0
3	B3LYP-D3/6-31+G(d),LANL2DZ (PCM,CH_2Cl_2) opt G09 (6D)	25.2	118.2	21.7	16.8	93.0
4	B3LYP-D3/6-31+G(d),LANL2DZ (PCM,CH_2Cl_2) SP G09 (5D)	9.4	102.4	5.9	1.1	93.0
5	B3LYP-D3/6-31+G(d),LANL2DZ (PCM,CH_2Cl_2) opt G16 (5D)	22.3	118.7	20.9	17.7	96.4
6	B3LYP-D3/6-31+G(d),GTBas1,LANL2DZ(PCM,CH_2Cl_2)SP G09(5D)	11.6	103.5	10.7	5.6	91.9
7	B3LYP-D3/6-31+G(d),def2-SVP (PCM,CH_2Cl_2) SP G09 (6D)	7.6	133.2	49.6	44.8	125.6
8	B3LYP-D3/def2-SVP (PCM,CH_2Cl_2) SP G09 (5D)	7.0	140.4	61.7	59.5	133.4
9	B3LYP-D3(BJ)/def2-SVP (PCM,CH_2Cl_2) SP G09 (5D)	5.3	140.8	69.4	68.0	135.5
10	B3LYP-D3(BJ)/def2-SVP (PCM,CH_2Cl_2) opt G09 (5D)	6.9	148.7	62.5	58.5	141.8
11	B3LYP-D3(BJ)/def2-TZVP (PCM,CH_2Cl_2) SP G09 (5D)	13.0	151.8	80.0	75.6	138.8
12	M06-2X/def2-SVP (PCM,SMD,CH_2Cl_2) SP G16 (5D)	20.1	212.6	77.7	76.0	192.5
13	M06-2X/def2-TZVP (PCM,SMD,CH_2Cl_2) SP G16 (5D)	27.1	226.2	89.1	83.8	199.1
14	ωB97XD/def2-TZVP (PCM,SMD,CH_2Cl_2) SP G16 (5D)	27.7	226.4	85.5	77.2	198.7
15	MP2/def2-TZVP (PCM,SMD,CH_2Cl_2) SP G16 (5D)	9.5	242.2	85.7	80.0	232.8
16	DLPNO-MP2/def2-TZVPP (CPCM,SMD) [b]	12.6	248.5	80.9	80.4	235.9
17	RI-SCS-MP2/def2-TZVPP (CPCM,SMD) [b]	22.5	246.0	75.1	73.5	223.5
18	DLPNO-CCSD(T)/def2-TZVPP (CPCM) [c]	15.9	217.8	40.3	36.3	201.9
19	DLPNO-CCSD(T)/def2-TZVPP (CPCM,SMD) [c]	22.4	255.9	72.6	72.4	233.5

[a] SI refers to energetics reported in the Supporting Information by Cossio and Vallribera[2]; 'opt' refers to results from optimized geometries at the listed level of theory, 'SP' refers to single-point energies calculated at the geometries reported by Cossio and Vallribera[2], converted to Δ*G* by the addition of G_{corr} from Cossio and Vallribera.[2] G09 and G16 refer to Gaussian 09 Rev E.01 and Gaussian 16 Rec C.01, respectively. 5D indicates that the 6-31+G(d) basis set uses pure d functions, whereas 6D indicates that the 6-31+G(d) basis set uses Cartesian d functions.

[b] CPCM with SMD solvation model. Calculated electronic energies at ωb97XD/def2-TZVP(PCM,SMD) optimized geometries. Δ*G* is the sum of the electronic energies and thermal correction (G_{corr}) calculated at the ωb97XD/def2-TZVP(PCM,SMD) level of theory.

[c] CPCM without SMD solvation model. Calculated electronic energies at ωb97XD/def2-TZVP(PCM,SMD) optimized geometries. Δ*G* is the sum of the electronic energies and thermal correction (G_{corr}) calculated at the ωb97XD/def2-TZVP(PCM,SMD) level of theory.

The first three rows (Table S2) reproduce the calculated energetics from Cossio and Vallribera.[2] The energies included in the SI of Ref. 2 can be reproduced exactly as shown in rows 2 and 3 (single-point energies and optimized geometries). There are some transcription errors from the SI data to Figure 1 in Ref. 2, however the SI data is correct and reproducible.

Comparison of Row 2 and 4 illustrates the impact of using pure (5d) functions (Row 4) in comparison with Cartesian (6d) functions (Row 2). The relative free energies are generally 10-15 kJ/mol smaller in magnitude with pure 5d functions in comparison with Cartesian 6d functions. By coincidence, the barrier height is the same when using pure d or Cartesian d functions.

Comparison of rows 2 and 7 illustrates the impact of the iodine basis set. Replacing the LANL2DZ basis and ECP with def2-SVP (ECP28MWB) results in the barrier increasing by 33 kJ/mol. Similarly, the relative free

energies of each component of the reaction are qualitatively different. The LANL2DZ basis and ECP is quite dated, and its use for modern computational work is not recommended.

The third set of results in Table S2 (rows 7-11) utilise the def2-SVP basis set. Here the barrier is calculated to be 125.6 to 141.8 kJ/mol. Similarly, results with M06-2X (rows 12-13) and ωB97XD (row 14) give a barrier of nearly 200 kJ/mol. Finally, in rows 15-19 the use of MP2 and CCSD(T) variants yields even higher barriers that exceed 200 kJ/mol. It is concluded that the B3LYP-D3/6-31+G(d),LANL2DZ calculated barrier is too low compared to higher-level calculations.

IRC calculations were carried out for TS1 identified by Cossio and Vallribera[2] (labelled TS2 in the present work) at the B3LYP-D3/6-31+G(d),LANL2DZ(PCM,CH_2Cl_2) level of theory. TS1 is clearly connected to RC1 (Figure S68, (a) reverse reaction). However, following the reaction coordinate in the opposite direction leads to an alternative structure that is different from Int1-anti and Int1-syn reported by Cossio and Vallribera.[2]

Following the IRC forward path, a newly optimized Int1new structure (Figure S69) was located that is in better agreement with the IRC results. The non-bonded Br atom lies in the plane of the anisole ring. Here Int1new (E_e = -5732.64333417 au, ΔG = -5732.47286 au) lies 41.0 kJ/mol higher in free energy than the reactants ($PhIBr_2$ + anisole).

(a) Reverse reaction (b) TS2 (c) Forward reaction

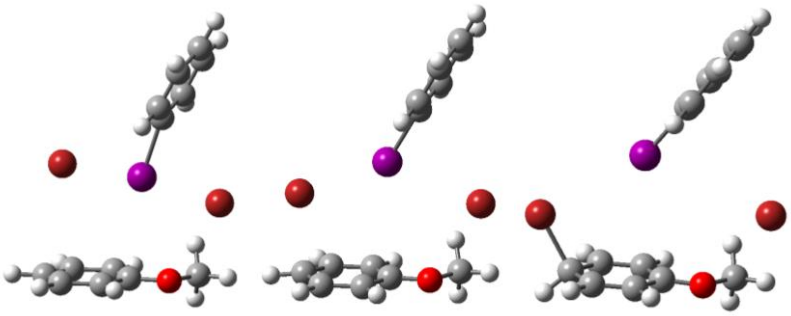

Figure S68: Results from IRC calculation (100 steps).

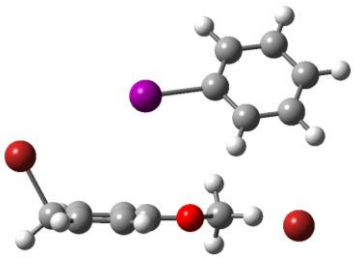

Figure S69: B3LYP-D3/6-31+G(d),LANL2DZ(PCM,CH_2Cl_2) optimized geometry of **Int1new**.

2.4 Reaction of $PhIBr_2$ and MeOPh (anisole)

We carried out a full investigation of the mechanism of $PhIBr_2$ + anisole at the ωB97X-D3(BJ)/def2-TZVP (CPCM, CH_2Cl_2) level of theory. Results and discussion are presented in the manuscript. Cartesian coordinates of all optimized geometries are provided below.

2.5 Optimised ωB97X-D3(BJ)/def2-TZVP (CPCM, CH_2Cl_2) Cartesian Coordinates (Å)

PhI

E_e = -529.639640411961 hartree

I	-0.00218400	-0.91631000	0.00000300
C	0.00221900	1.17027600	0.00000000
C	0.00830100	3.93889100	-0.00000100
C	0.00064100	1.85177700	1.21058800
C	0.00675500	1.85176300	-1.21058800
C	0.00981100	3.24256200	-1.20348100
C	0.00372600	3.24257700	1.20347900
H	-0.00294200	1.30780200	2.14762800
H	0.00790600	1.30777600	-2.14762700
H	0.01340400	3.78079700	-2.14519700
H	0.00254300	3.78082300	2.14519500
H	0.01071200	5.02334800	-0.00000200

Br_2

E_e = -5148.1298211612 hartree

Br	0.00000000	0.00000000	1.13769800
Br	0.00000000	0.00000000	-1.13769800

RC1

E_e = -5677.7747656734 hartree

I	-0.43619000	-0.33607600	-1.82829600
C	0.33683700	0.37078700	-0.02676600
C	1.58184900	0.98642400	-0.01277300
C	2.08497100	1.46798200	1.19073500
C	1.35005200	1.33254400	2.36343300
C	0.10669300	0.71052000	2.33410400
C	-0.40825400	0.22642200	1.13647500
H	-1.37878100	-0.25460600	1.11090800
H	-0.47032800	0.59962500	3.24576300
H	1.74643400	1.71068100	3.29930800
H	3.05500600	1.95310400	1.20685800
H	2.14996500	1.09786800	-0.92852500
Br	-2.13861300	3.28524400	-0.56855800
Br	-0.18705600	3.70138000	-1.65533200

TS1

E_e = -5677.69109717658 hartree

I	-0.33359600	-1.53853900	-2.44559200
C	0.09534500	-0.65424900	-0.63584000
C	1.30571100	0.01943600	-0.49357700
C	1.58863600	0.61696500	0.72627500
C	0.67471500	0.53510200	1.77347300
C	-0.52856100	-0.14372900	1.60995000
C	-0.83272100	-0.74390600	0.39561000
H	-1.77374200	-1.25760100	0.24900400
H	-1.23883600	-0.20163200	2.42684400
H	0.90245100	1.00500300	2.72384700
H	2.52520600	1.14660500	0.85826100
H	2.00844100	0.07436700	-1.31600100
Br	-3.23703100	0.40997600	-1.97466200
Br	-1.15601800	0.73220200	-3.89759300

Int1

E_e = -5677.7356927259 hartree

I	-0.39026200	-1.18084500	-2.56574300
C	0.10014000	-0.43750700	-0.70381300
C	1.42025700	-0.06407400	-0.47350900
C	1.74265600	0.41195500	0.78817600
C	0.76157700	0.49966900	1.77266200
C	-0.55055300	0.12024000	1.50931900
C	-0.90398600	-0.35546000	0.25297600
H	-1.92497100	-0.63309200	0.01207100
H	-1.30714600	0.19522500	2.28174900
H	1.02451300	0.87088800	2.75698100
H	2.76145500	0.71412600	1.00018800
H	2.16838400	-0.14083600	-1.25300000
Br	-3.99681200	-0.89664700	-1.66505800
Br	-0.90525300	0.89635900	-3.71299600

TS2

E_e = -5677.73481123935 hartree

I	-0.53726300	-0.99793500	-2.59948800
C	0.03164000	-0.33579200	-0.72734000
C	1.38578200	-0.12452700	-0.48940800
C	1.75526900	0.28398400	0.78301400
C	0.78677400	0.45706100	1.76971000
C	-0.55874300	0.23217000	1.49851300
C	-0.96030200	-0.16665600	0.22958100
H	-2.00144400	-0.36283800	-0.00708700
H	-1.30323000	0.36422500	2.27492800
H	1.08765200	0.76838500	2.76391100
H	2.80096300	0.46127200	1.00545300
H	2.12310300	-0.27207500	-1.26898000
Br	-4.04907000	-1.41605000	-1.41645900
Br	-0.56113200	1.10877600	-3.81634800

$PhIBr_2$

E_e = -5677.77917335913 hartree

I	-0.54426000	0.35356400	-1.80120000
C	0.33917600	0.66981800	0.05782200
C	1.42665600	1.52447400	0.13172400
C	2.02258600	1.70887600	1.37367400
C	1.52371700	1.05188000	2.49387200
C	0.42569900	0.20471900	2.38615500
C	-0.18220700	0.00102500	1.15306300
H	-1.03774800	-0.65591700	1.05350100
H	0.03976700	-0.30532900	3.26127700
H	1.99483400	1.20080700	3.45903200
H	2.87791700	2.36891200	1.46202300
H	1.80710700	2.02576700	-0.74989300
Br	-2.57081300	1.83472600	-1.02546600
Br	1.54017800	-1.10223300	-2.45037200

Anisole

E_e = -347.052061526436 hartree

C	0.92024100	-0.50843500	-0.00000300
C	0.46450700	-1.82603200	-0.00000100
C	-0.89182700	-2.11452200	0.00000100
C	-1.80900400	-1.06413900	0.00000100
C	-1.37322100	0.24996900	-0.00000100
C	-0.00456200	0.53309500	-0.00000300
H	1.19096300	-2.63212700	-0.00000100
H	-1.23519500	-3.14290100	0.00000400

H	-2.87400100	-1.27197100	0.00000200
H	-2.07749800	1.07484900	-0.00000100
O	0.33045500	1.85318700	-0.00000300
H	1.98418000	-0.31198700	-0.00000400
C	1.71459300	2.18296900	0.00000100
H	1.76489600	3.27062700	0.00000300
H	2.21166400	1.79327100	0.89350500
H	2.21167000	1.79327400	-0.89350100

RC2

E_e = -6024.84344631234 hartree

C	3.50188400	-0.04568300	-0.42045500
C	3.22803000	0.56243500	0.81424100
C	2.66349400	1.84715500	0.83966000
C	2.36215600	2.52410600	-0.34430100
C	2.63347600	1.90396300	-1.57270700
C	3.19872200	0.63143700	-1.61451700
H	3.44308500	0.05599400	1.74781000
H	2.45041600	2.30945300	1.80008000
H	1.90699600	3.50851700	-0.31269000
H	2.39604700	2.41304900	-2.50315000
H	3.40972400	0.13951300	-2.55959600
O	4.06617300	-1.27839200	-0.56644900
C	4.39552700	-2.02330900	0.60778700
H	4.81645000	-2.96435900	0.25070500
H	3.49967300	-2.22600600	1.20553200
H	5.14167300	-1.49357600	1.21358700
Br	-1.33051100	2.77070900	0.27899600
I	-0.34236600	0.16120400	0.22376200
Br	0.64372900	-2.44310900	0.16775300
C	-2.32257400	-0.58069700	-0.10921200
C	-3.10081000	-0.91241900	0.99753600
C	-4.39299800	-1.39407500	0.76502600
C	-4.87194100	-1.52893500	-0.54231200
C	-4.06368000	-1.18545700	-1.63104500
C	-2.76741700	-0.70348800	-1.42351000
H	-2.72545200	-0.80553100	2.00921200
H	-5.01984500	-1.66091400	1.61077500
H	-5.87722300	-1.90276100	-0.71300400
H	-4.43473300	-1.28992800	-2.64633000
H	-2.13663100	-0.43629500	-2.26406300

TS3

E_e = -6024.80140273801 hartree

C	3.38405300	1.92910200	0.16420100
C	3.02738800	1.47979000	-1.12196800
C	2.38114400	0.27683500	-1.24966500
C	2.01689800	-0.49368700	-0.11070900
C	2.46968700	-0.05302400	1.16972400
C	3.11989200	1.13708000	1.30625800
H	3.24868100	2.07067300	-1.99929000
H	2.09966500	-0.08147300	-2.23347500
H	1.72125100	-1.52759100	-0.24323600
H	2.25209500	-0.66104400	2.04032600
H	3.43325800	1.50826700	2.27431400
O	3.97936500	3.08802500	0.40169900
C	4.24332700	3.97828700	-0.69474300
H	4.70096000	4.85779000	-0.24898000
H	3.30957600	4.25061000	-1.19070000
H	4.93259000	3.51489200	-1.40300800
Br	-0.14148000	0.35010800	0.02147400
I	-2.62497700	1.38280000	0.19485400
Br	-0.92751100	4.06483400	0.21395800
C	-3.55936500	-0.48763000	0.12762900
C	-3.87577400	-1.04057800	-1.10772800
C	-4.49438200	-2.28473200	-1.15038000
C	-4.78968200	-2.95977900	0.02952300
C	-4.46589500	-2.39459500	1.25858400
C	-3.84562300	-1.15142900	1.31452200
H	-3.64313200	-0.51008100	-2.02404000
H	-4.74653500	-2.72511100	-2.10880100
H	-5.27415500	-3.92932300	-0.00895100
H	-4.69633200	-2.92032400	2.17869800
H	-3.58949100	-0.70673500	2.26934800

Int2

E_e = -6024.8216357104 hartree

C	3.25574100	0.34081100	-1.33421700
C	3.13695900	-0.61133000	-0.20524800
C	3.19665600	-0.01129400	1.14868400
C	3.32814700	1.30594500	1.33065600
C	3.41321900	2.18124800	0.18883300
C	3.36794400	1.66265900	-1.15310900
Br	1.39831200	-1.50095300	-0.38255200
O	3.61868300	3.41632900	0.46621100
C	3.64003500	4.42468900	-0.57829700
Br	0.33014100	2.86876500	-0.09859700
I	-2.20624900	0.57206000	0.02386600
C	-3.77731000	-0.80814700	0.08380000
C	-4.27586700	-1.23543800	1.30973200
C	-5.32265600	-2.15077800	1.34336800
C	-5.86925400	-2.63588400	0.16037800
C	-5.36540700	-2.20240900	-1.06110800
C	-4.31861200	-1.28761600	-1.10421000
H	3.86589200	-1.41888800	-0.30401200
H	-3.85248000	-0.85705800	2.23308300
H	-3.92852300	-0.95005600	-2.05764100
H	-5.78777300	-2.57475100	-1.98839900
H	-5.71139200	-2.48251500	2.30033900
H	-6.68630700	-3.34857200	0.19004500
H	3.23149500	-0.07893500	-2.33345000
H	3.12181500	-0.68744100	1.99262000
H	3.36905900	1.75934000	2.31284400
H	3.43143100	2.33696100	-1.99450600
H	3.77547100	5.36425600	-0.05141100
H	4.47492200	4.23374300	-1.25128700
H	2.68143500	4.40110200	-1.09548000

***p*-bromo anisole**

E_e = -2920.52025968472 hartree

C	0.92152200	-0.50510900	-0.00001900
C	0.47921200	-1.82611100	-0.00000900
C	-0.87593600	-2.09888700	0.00000500
C	-1.81058300	-1.06922400	0.00000200

C	-1.37375300	0.24299400	-0.00000900
C	-0.00633900	0.53368500	-0.00001600
H	1.20093800	-2.63420400	-0.00000800
H	-2.87112000	-1.29073500	0.00001100
H	-2.08479900	1.06148300	-0.00000700
O	0.32169500	1.85141100	-0.00001800
H	1.98521400	-0.30901600	-0.00002700
C	1.70541200	2.18907400	0.00001000
H	1.74851700	3.27678100	0.00002000
H	2.20276700	1.80172200	0.89409200
H	2.20280200	1.80173800	-0.89406000
Br	-1.47273000	-3.89783400	0.00003500

HBr

E_e = -2574.6771561447 hartree

Br	0.00000000	0.00000000	0.71032500
H	0.00000000	0.00000000	-0.71032500

PhI(OTFA)$_2$

E_e = -1582.58833037731 hartree

I	-0.00048100	0.62759300	-0.00105400
C	-0.29778900	-3.49026500	-1.17184600
C	-0.29616900	-2.10102000	-1.18419900
C	-0.00017700	-1.44136800	-0.00105100
C	0.29618900	-2.10070100	1.18219700
C	0.29854800	-3.48993700	1.17005900
C	0.00055100	-4.17916500	-0.00084500
H	-0.52895400	-4.03170500	-2.08192100
H	-0.52253800	-1.55169400	-2.08998100
H	0.52237600	-1.55115100	2.08788600
H	0.53003300	-4.03112700	2.08020100
H	0.00082600	-5.26343000	-0.00075900
O	-2.11827000	0.35412900	-0.01365800
O	2.11702200	0.35456100	0.01078100
C	-2.76110800	1.47528500	-0.08964100
O	-2.28393500	2.58659800	-0.12082800
C	2.76059000	1.47505400	0.09096400
O	2.28427400	2.58655700	0.12617200
C	-4.29938700	1.25092400	-0.12395100
F	-4.63147400	0.34332100	-1.05185900
F	-4.72680900	0.80093600	1.06616100
F	-4.94598000	2.38246400	-0.39802300
C	4.29860400	1.24878900	0.12550400
F	4.62854900	0.34112800	1.05418300
F	4.72611400	0.79750800	-1.06403400
F	4.94675000	2.37946300	0.39936700

TMSBr

E_e = 2983.56324218779 hartree

C	-0.18864100	-0.80152300	-0.53038400
C	-1.57284200	-0.27933700	-3.23823900
C	-0.50376700	2.09417200	-1.56560300
H	-0.05414800	-0.42981600	0.48808300
H	-0.66239800	-1.78514700	-0.48544200
H	0.79747400	-0.91361000	-0.99239100
H	-2.24045800	0.39169300	-3.78372900
H	-0.63682800	-0.36917300	-3.79896600
H	-2.03701500	-1.26682100	-3.18135000
H	0.46947800	2.08095300	-2.06621500
H	-1.16303300	2.77721700	-2.10647100
H	-0.36521600	2.47132200	-0.54949700
Si	-1.21395800	0.37704300	-1.53685200
Br	-3.21231700	0.54327700	-0.47705000

TMS-OTFA

E_e = -935.989805084434 hartree

C	0.02726400	-0.00061200	-0.00724600
C	-0.02868900	0.00522300	1.54297200
O	1.17802400	0.00661600	2.04335500
Si	1.53251100	0.00489300	3.74500100
C	0.81362700	-1.54717500	4.46319900
H	1.18265400	-2.42771500	3.93032800
H	1.11342700	-1.63429100	5.51201100
H	-0.27718400	-1.53861700	4.41645700
H	1.18443600	2.43756600	3.93823800
H	-0.27656500	1.54764400	4.42071700
H	1.11385500	1.63871000	5.51734900
C	3.38668300	0.00455600	3.75424200
H	3.78075000	0.89364900	3.25523700
H	3.75039400	0.00184600	4.78605800
H	3.78017500	-0.88223900	3.25070200
O	-1.07490700	0.00743400	2.13455500
C	0.81437700	1.55535600	4.46794600
F	-1.19512600	-0.00746900	-0.53524100
F	0.67341000	1.08542500	-0.45682600
F	0.68175300	-1.08505000	-0.44843800

PhI(OTFA)Br

E_e = -3630.18417270785 hartree

C	3.29952700	-1.43502700	-2.94858800
O	1.52482800	0.10637100	-2.82738800
I	-0.43883900	0.81584800	-2.10903500
C	0.48925500	0.84658800	-0.25261100
C	1.33147500	1.90890000	0.03949800
C	1.98339400	1.90058300	1.26676600
C	1.78111000	0.85200700	2.15832200
C	0.92692300	-0.19774600	1.83628200
C	0.26695600	-0.21264000	0.61350000
H	-0.39231300	-1.02780500	0.34294900
H	0.77643600	-1.01434100	2.53300100
H	2.29554400	0.85204200	3.11280600
H	2.65120200	2.71521900	1.52252200
H	1.48194100	2.71626300	-0.66696600
O	1.15097900	-1.96064800	-2.00996600
C	1.83051400	-1.11421900	-2.54680900
Br	-2.57722800	1.79033700	-1.10144100
F	4.14549500	-0.73428700	-2.17219600
F	3.58004000	-2.73058800	-2.79610000
F	3.54621300	-1.10573000	-4.22489800

OTFA-Br

E_e = -3100.51213077381 hartree

C	-0.03769200	0.00007900	-0.11062100
C	-0.00416600	-0.00000600	1.44512000

O	1.27423100	-0.00014700	1.82778300	F	0.57758200	1.08464600	-0.59235600
O	-0.97909000	0.00006500	2.12708500	F	0.57765400	-1.08437800	-0.59250600
Br	1.55690900	-0.00018500	3.62992000				
F	-1.29524400	0.00006900	-0.53545200				

References

1. Seecharan, V.; Armand, L.; Noorollah, J.; Singh, N.; Zhang, A.; Freddo, K. P.; Spatola, N.; Prasad, S.; Chaudhry, A.; War, S. W.;Hyatt, I.F. D.; Silverio, D. L., Ligand exchange of aryl iodine dicarboxylates to form reagents with differing solubilities. *Arkivoc* **2020,** (part iv), 79-85.
2. Granados, A.; Shafir, A.; Arrieta, A.; Cossio, F. P.; Vallribera, A., Stepwise mechanism for the bromination of arenes by a hypervalent iodine reagent. *J. Org. Chem.* **2020,** *85*, 2142-2150.
3. Fryberg, M.; Oehlschlager, A. C.; Unrau, A. M., The synthesis of possible polyene intermediates in phytosterol biosynthesis. *Tetrahedron* **1971,** *27*, 1261-1274.
4. Karade, N.; Shirodkar, S.; Dhoot, B.; Waghmare, P., An efficient and mild direct oxidative methyl esterification of aromatic aldehydes using NaBr and diacetoxyiodobenzene. *J. Chem. Res.* **2005,** *2005* (4), 274-276.
5. Watanabe, A.; Koyamada, K.; Miyamoto, K.; Kanazawa, J.; Uchiyama, M., Decarboxylative Bromination of Sterically Hindered Carboxylic Acids with Hypervalent Iodine (III) Reagents. *Org. Process Res. & Dev.* **2020,** *24* (7), 1328-1334.
6. Frank, A.; Seel, C. J.; Groll, M.; Gulder, T., Characterization of a cyanobacterial haloperoxidase and evaluation of its biocatalytic halogenation potential. *ChemBioChem* **2016,** *17* (21), 2028-2032.
7. Oberhauser, T., A New Bromination Method for Phenols and Anisoles: NBS/HBF (4). Et (2) O in CH (3) CN. *J. Org. Chem.* **1997,** *62* (13), 4504-4506.
8. Mo, F.; Yan, J. M.; Qiu, D.; Li, F.; Zhang, Y.; Wang, J., Gold-Catalyzed Halogenation of Aromatics by N-Halosuccinimides. *Angew. Chem. Int. Ed.* **2010,** *49* (11), 2028-2032.
9. Neese, F., The ORCA program system. *WIREs Comp. Mol. Sci.* **2012,** *2* (1), 73-78.
10. Weigend, F.; Ahlrichs, R., Balanced basis sets of split valence, triple zeta valence and quadruple zeta valence quality for H to Rn: Design and assessment of accuracy. *Phys. Chem. Chem. Phys.* **2005,** *7* (18), 3297-3305.
11. Peterson, K. A.; Figgen, D.; Goll, E.; Stoll, H.; Dolg, M., Systematically convergent basis sets with relativistic pseudopotentials. II. Small-core pseudopotentials and correlation consistent basis sets for the post-d group 16–18 elements. *J. Chem. Phys.* **2003,** *119* (21), 11113-11123.
12. Weigend, F., Accurate Coulomb-fitting basis sets for H to Rn. *Phys. Chem. Chem. Phys.* **2006,** *8* (9), 1057-1065.
13. Hellweg, A.; Hättig, C.; Höfener, S.; Klopper, W., Optimized accurate auxiliary basis sets for RI-MP2 and RI-CC2 calculations for the atoms Rb to Rn. *Theor. Chem. Acc.* **2007,** *117* (4), 587-597.
14. Barone, V.; Cossi, M., Quantum Calculation of Molecular Energies and Energy Gradients in Solution by a Conductor Solvent Model. *J. Phys. Chem. A* **1998,** *102* (11), 1995-2001.
15. Ásgeirsson, V.; Birgisson, B. O.; Bjornsson, R.; Becker, U.; Neese, F.; Riplinger, C.; Jónsson, H., Nudged Elastic Band Method for Molecular Reactions Using Energy-Weighted Springs Combined with Eigenvector Following. *J. Chem. Theor. Comp.* **2021,** *17* (8), 4929-4945.
16. Frisch, M. J.; Trucks, G. W.; Schlegel, H. B.; Scuseria, G. E.; Robb, M. A.; Cheeseman, J. R.; Scalmani, G.; Barone, V.; Mennucci, B.; Petersson, G. A.; Nakatsuji, H.; Caricato, M.; Li, X.; Hratchian, H. P.; Izmaylov, A. F.; Bloino, J.; Zheng, G.; Sonnenberg, J. L.; Hada, M.; Ehara, M.; Toyota, K.; Fukuda, R.; Hasegawa, J.; Ishida, M.; Nakajima, T.; Honda, Y.; Kitao, O.; Nakai, H.; Vreven, T.; J. A. Montgomery, J.; Peralta, J. E.; Ogliaro, F.; Bearpark, M.; Heyd, J. J.; Brothers, E.; Kudin, K. N.; Staroverov, V. N.; Kobayashi, R.; Normand, J.; Raghavachari, K.; Rendell, A.; Burant, J. C.; Iyengar, S. S.; Tomasi, J.; Cossi, M.; Rega, N.; Millam, J. M.; Klene, M.; Knox, J. E.; Cross, J. B.; Bakken, V.; Adamo, C.; Jaramillo, J.; Gomperts, R.; Stratmann, R. E.; Yazyev, O.; Austin, A. J.; Cammi, R.; Pomelli, C.; Ochterski, J. W.; Martin, R. L.; Morokuma, K.; Zakrzewski, V. G.; Voth, G. A.; Salvador, P.; Dannenberg, J. J.; Dapprich, S.; Daniels, A. D.; Farkas, Ö.; Foresman, J. B.; Ortiz, J. V.; Cioslowski, J.; Fox, D. J. *Gaussian 09, Revision E.01*, Gaussian 09, Revision E.01, Gaussian, Inc.: Wallingford CT, 2013.
17. Frisch, M. J.; Trucks, G. W.; Schlegel, H. B.; Scuseria, G. E.; Robb, M. A.; Cheeseman, J. R.; Scalmani, G.; Barone, V.; Petersson, G. A.; Nakatsuji, H.; Li, X.; Caricato, M.; Marenich, A. V.; Bloino, J.; Janesko, B. G.; Gomperts, R.; Mennucci, B.; Hratchian, H. P.; Ortiz, J. V.; Izmaylov, A. F.;

Sonnenberg, J. L.; Williams-Young, D.; Ding, F.; Lipparini, F.; Egidi, F.; Goings, J.; Peng, B.; Petrone, A.; Henderson, T.; Ranasinghe, D.; Zakrzewski, V. G.; Gao, J.; Rega, N.; Zheng, G.; Liang, W.; Hada, M.; Ehara, M.; Toyota, K.; Fukuda, R.; Hasegawa, J.; Ishida, M.; Nakajima, T.; Honda, Y.; Kitao, O.; Nakai, H.; Vreven, T.; Throssell, K.; Montgomery Jr., J. A.; Peralta, J. E.; Ogliaro, F.; Bearpark, M. J.; Heyd, J. J.; Brothers, E. N.; Kudin, K. N.; Staroverov, V. N.; Keith, T. A.; Kobayashi, R.; Normand, J.; Raghavachari, K.; Rendell, A. P.; Burant, J. C.; Iyengar, S. S.; Tomasi, J.; Cossi, M.; Millam, J. M.; Klene, M.; Adamo, C.; Cammi, R.; Ochterski, J. W.; Martin, R. L.; Morokuma, K.; Farkas, O.; Foresman, J. B.; Fox, D. J. *Gaussian 16 Rev. E.01*, Wallingford, CT, 2016.

18. McGrath, M. P.; Radom, L., Extension of Gaussian-1 (G1) theory to bromine-containing molecules. *J. Chem. Phys.* **1991,** *94* (1), 511-516.

19. Rassolov, V. A.; Ratner, M. A.; Pople, J. A.; Redfern, P. C.; Curtiss, L. A., 6-31G* basis set for third-row atoms. *J. Comp. Chem.* **2001,** *22* (9), 976-984.

20. Riplinger, C.; Pinski, P.; Becker, U.; Valeev, E. F.; Neese, F., Sparse maps—A systematic infrastructure for reduced-scaling electronic structure methods. II. Linear scaling domain based pair natural orbital coupled cluster theory. *J. Chem. Phys.* **2016,** *144* (2), 024109.

21. Riplinger, C.; Neese, F., An efficient and near linear scaling pair natural orbital based local coupled cluster method. *J. Chem. Phys.* **2013,** *138* (3), 034106.

22. Pinski, P.; Neese, F., Analytical gradient for the domain-based local pair natural orbital second order Møller-Plesset perturbation theory method (DLPNO-MP2). *J. Chem. Phys.* **2019,** *150* (16), 164102.

23. Pinski, P.; Neese, F., Exact analytical derivatives for the domain-based local pair natural orbital MP2 method (DLPNO-MP2). *J. Chem. Phys.* **2018,** *148* (3), 031101.

24. Grimme, S., Improved second-order Møller–Plesset perturbation theory by separate scaling of parallel- and antiparallel-spin pair correlation energies. *J. Chem. Phys.* **2003,** *118* (20), 9095-9102.

25. Marenich, A. V.; Cramer, C. J.; Truhlar, D. G., Universal Solvation Model Based on Solute Electron Density and on a Continuum Model of the Solvent Defined by the Bulk Dielectric Constant and Atomic Surface Tensions. *J. Phys. Chem. B* **2009,** *113* (18), 6378-6396.